12-2016

The Coronary Circulation in an *In Vitro* Multi-Scale Model of the Stage 1 Norwood Procedure

Lauren Elizabeth Carter
Clemson University

THE CORONARY CIRCULATION IN AN *IN VITRO* MULTI-SCALE MODEL OF THE STAGE 1 NORWOOD PROCEDURE

A Thesis
Presented to
the Graduate School of
Clemson University

In Partial Fulfillment
of the Requirements for the Degree
Master of Science
Mechanical Engineering

---

by
Lauren Elizabeth Carter
November 2016

Accepted by:
Dr. Richard Figliola, Committee Chair
Dr. Donald Beasley, Committee Member
Dr. Tiffany Camp, Committee Member
Dr. Ethan Kung, Committee Member

ABSTRACT

Hypoplastic Left Heart Syndrome (HLHS) is a congenital heart disease where the left ventricle and ascending aorta are underdeveloped. The first of three palliative surgeries for this malformation is the Norwood procedure. In this surgery, an opening is made between the left and right atrium so that all blood can flow into the right ventricle (RV). A reconstructed aorta is anastomosed (connected) to the RV so that the RV can pump oxygenated blood to the body (the systemic circulation). To divert part of the systemic blood flow to the pulmonary circulation, the modified Blalock-Taussig Shunt (mBTS) is connected from the innominate artery to the pulmonary artery. However, Norwood patients with an mBTS may experience retrograde flow from the coronary circulation (which supplies blood to the heart) to the pulmonary circulation via the mBTS. This shunt steal of coronary blood can lead to detrimental issues such as myocardial ischemia leading to right ventricular dysfunction.

In this study, a multi-scale model of the Norwood procedure couples a three-dimensional (3D) test section of the reconstructed aortic arch with a lumped parameter network (LPN) describing the Norwood patient's global hemodynamics. Previously, only *in silico* multi-scale models of the Norwood circulation have modeled the coronary circulation and the effects of varying mBTS sizes on coronary perfusion. Here, a novel *in vitro* coronary circulation model is adapted from such *in silico* studies and implemented into a previously validated *in vitro* mock circulatory system (MCS) of the Norwood with mBTS palliation. The MCS was verified against an analytical model and validated using

a patient-specific test section and data. A parametric test in which the size of the mBTS inner diameter was varied from 3mm to 4mm was performed. The results showed that increasing mBTS size results in decreased diastolic aortic pressure, which decreases coronary blood flow (CBF) during diastole.

ACKNOWLEDGEMENTS

I am thankful for the many people and organizations that have made this thesis possible. Special thanks are given to the following:

Thank you to the Leducq Foundation for supporting my work and me financially.

To my research advisor and professor, Dr. Richard Figliola: Thank you for always letting me barge into your office with questions and ideas. I have taken all of your advice and shared knowledge to heart, and I will be forever grateful for the honor and privilege of working under your guidance.

Thank you to my committee members, Dr. Ethan Kung, Dr. Donald Beasley, and Dr. Tiffany Camp, for your support and interest in my work.

Thank you to Dr. Chiara Corsini, Dr. Catriona Baker, Dr. Francesco Migliavacca, and Dr. Giovanni Biglino for your support and answering all of my questions.

Thank you to my research team/family: Dr. Tim Conover, Dr. Chad Smith, Dr. Tian-qi Hang, Dr. Jian Zhou, Laura Chopp, and Will Becker. In particular, thank you Tim for your time and effort in helping to develop this model. Thank you Chad for always taking your time to share your expertise and be a friendly face in the lab.

Thank you to my caring and supportive friend, Phoebe Bickford. To say “I wouldn’t have made it through my undergraduate and graduate studies without you” is the understatement of the century.

Lastly, I thank my family: Mom, Dad, Meredith Ann, and Jim, for your love, support, and unending belief in me. If ever I was in doubt or frustrated, you are the reason I kept working.

TABLE OF CONTENTS

Page

LIST OF TABLES

Table Page

LIST OF FIGURES

Figure Page

NOMENCLATURE

Arterial Coronary Blood Flow	Q_{cor}	Left Ventricle	LV
Atrium	Atr	Lower Body	LB
Beats Per Minute	bpm	Lumped Parameter Network	LPN
Body Surface Area	BSA	Mock Circulatory System	MCS
Cardiac Output	CO, Q_{AO}	modified Blalock-Taussig Shunt	mBTS
C_{cb}-SVP Coupling Chamber	CC	Myocardial Oxygen Supply-Demand Balance	MOB
Central Shunt	CS	Patent Ductus Arteriosus	PDA
Coarctation	COA	Pressure	P
Compliance, Capacitance	C	Pulmonary Artery	PA
Coronary Blood Flow	CBF	Pulmonary Vascular Resistance	PVR
Coronary Perfusion Pressure	CPP	Pulmonary-to-Systemic Blood Flow	Q_p/Q_s
Damus-Kaye-Stansel	DKS	Resistance	R
Data Acquisition System	DAQ	Right Atrium	RA
Diastolic Pressure Time Index	DPTI	Right Coronary Artery	RCA
Endocardial Viability Ratio	EVR	Right Ventricle	RV
Flow	Q	Single Ventricle Pressure	SVP
Heart Rate	HR	Systemic Vascular Resistance	SVR
Hypoplastic Left Heart Syndrome	HLHS	Tension Time Index	TTI
Inertance	L	Three-dimensional	3D
Innominate Artery	INOM	Upper Body	UB
Intramyocardial Pump	IMP	Venous Coronary Blood Flow	Q_{CV}
Left Atrium	LA	Ventricular Assist Device	VAD
Left Carotid Artery	LCA	Ventricular Power	VP
Left Subclavian Artery	LSA	Zero-dimensional	0-D

CHAPTER ONE

THE NORWOOD PROCEDURE AND CORONARY CIRCULATION

Hypoplastic Left Heart Syndrome

Every year there are approximately 10 in 10,000 children born with Hypoplastic Left Heart Syndrome [1]. Although rare, this congenital disease is one of the deadliest and attributes to 20% of the heart-related deaths in newborns per year [1]. The HLHS physiology is marked by a severely underdeveloped left ventricle (LV) and aorta that are unable to support the systemic circulation: the blood flow that provides oxygen to the body. Other characteristics of this disease may include aortic valve or mitral valve stenosis [2]: narrowing that further hinders the blood flow through the left side of the heart. A full anatomical representation of the HLHS heart relative to a normal healthy heart can be seen in Figure 1.1.

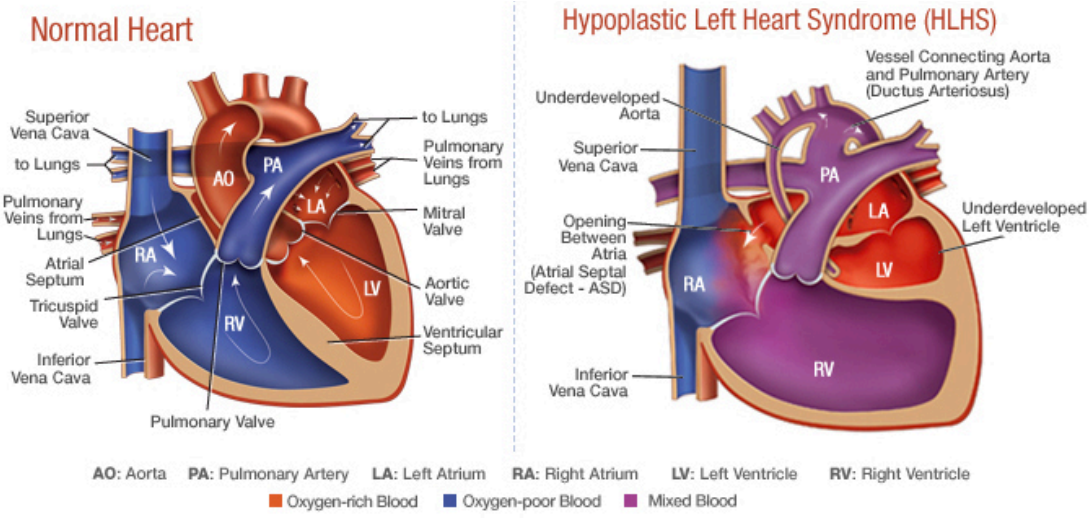

Figure 1.1 Anatomy of a normal heart (Left) and a heart with HLHS (Right). [3]

As seen in Figure 1.1, the hypoplastic LV's size greatly limits its ability to provide oxygenated blood to the systemic circulation. At birth, the patent ductus arteriosus (PDA) connects the pulmonary artery to the aortic arch, providing oxygenated blood to the systemic circulation. However, the PDA will close within a few weeks after birth and, unless medically intervened, the disease is fatal [4]. Symptoms of HLHS include fatigue or cyanosis: where the patient's skin tone appears blue, a mark of oxygen insufficiency [4]. This alerts doctors to perform medical imaging techniques such as echocardiography, and from there HLHS can be diagnosed. Once diagnosed, reconstruction of the heart is performed within 2-5 days of the patient's life. [4]

HLHS patients are treated with a set of 3 palliative surgeries: the Norwood, Glenn, and Fontan. The Norwood procedure (Stage 1) and its many variations occur within the first few days of birth. The Glenn procedure (Stage 2) occurs within 4-6 months. The previous surgeries are all performed with the end goal to create the Fontan circulation, marked by the total cavo-pulmonary connection [5]. This is the Fontan procedure (Stage 3) and occurs when the patient is 2-6 years old [4]. Overall, the survival rate to adulthood for these patients is limited, particularly with 5-30% mortality after Stage 1 [4, 6]. Due to these high rates, the Norwood procedure continues to be a topic of research in hopes of discovering new methods or optimizing the current palliative method.

Stage 1 Anatomy and Physiology

The purpose of the Norwood procedure is to provide both systemic and pulmonary blood flow [7]. To do this, a neo-aorta is constructed using the hypoplastic ascending aorta and a homograft patch, and anastomosed (connected) to the pulmonary trunk. The native aortic trunk may then be anastomosed to the neo-aorta by means of the Damus-Kaye-Stansel (DKS) procedure. In this configuration, the RV now acts as the systemic ventricle and pumps blood into the neo-aorta to the systemic circulations: upper body, lower body, and coronary circulations. The RV receives both oxygenated and deoxygenated blood from the right atrium (RA) and the left atrium (LA) via the atrial septal defect: an opening between the RA and LA.

The trademark of Stage 1 is the means by which it diverts part of the blood flow back to the pulmonary arteries (PA) to be oxygenated in the lungs. This is achieved using a shunt such as the modified Blalock-Taussig shunt (mBTS). Figure 1.2 shows the Stage 1 with mBTS palliation of a HLHS heart.

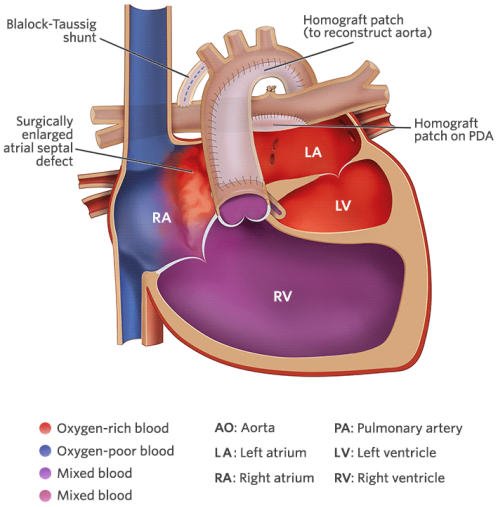

Figure 1.2 Anatomy of the Stage 1 with mBTS palliation for HLHS. [3]

The mBTS is a polytetrafluorethylene conduit from the innominate artery (INOM) or subclavian artery to the left or right PA [6]. When blood is pumped from the RV, it travels up through the aorta into the systemic arteries, including the INOM. As blood passes through the INOM, it can then pass through the mBTS to the PA. This completes the parallel systemic and pulmonary circulation [7] of the Norwood physiology, which is in contrast to a series circulation for a normal patient.

From Figure 1.2, it can be seen that the RV is the main pumping mechanism for the Norwood heart. It provides the flow of blood into the ascending aorta, the cardiac output (CO), which is used to perfuse both the systemic and pulmonary circulations. As indicated by Figure 1.2, the CO is mixed with both oxygen-rich and oxygen-poor blood. Placement and size of the mBTS is chosen in order to provide a proper balance of pulmonary-to-systemic blood flow (Q_P/Q_S) [8]. This is necessary to ensure that correct blood-oxygen saturation rates are met.

The mBTS's performance is highly dependent on the pulmonary vascular resistance (PVR), which is much smaller relative to the systemic vascular resistance (SVR), and changes with patient growth [9]. *In vitro* studies have found that a ratio of about 1:1 for Q_p/Q_S using a mBTS with a diameter of 3.5 mm is optimal for systemic oxygenation [8-9]. While achieving this balance is possible, the mBTS is still marked by complications. Most notably, the mBTS has been associated with "shunt steal": diastolic flow into the mBTS from retrograde flow in the systemic arteries [10]. In particular, this

diastolic runoff into the pulmonary circulation has been associated with detriment to the flow of blood in the coronary circulation. [6, 10–12]

Coronary Arteries for the Healthy Heart

The heart can be thought of as a pump whose energy source is oxygenated blood traveling through the coronary circulation. In a healthy heart, the coronary circulation is composed of coronary arteries that originate at the two ostia located in the aortic sinuses behind the aortic valve, as seen in Figure 1.3 below. From there, the left (LCA) and right (RCA) coronary arteries spread over the outer epicardium and descend into the inner myocardium and innermost endocardium of the left and right ventricles, respectively. This blood flow provides the oxygen the heart muscle needs for contraction during systole. The deoxygenated blood is then directed through coronary veins that empty into the RA. [13]

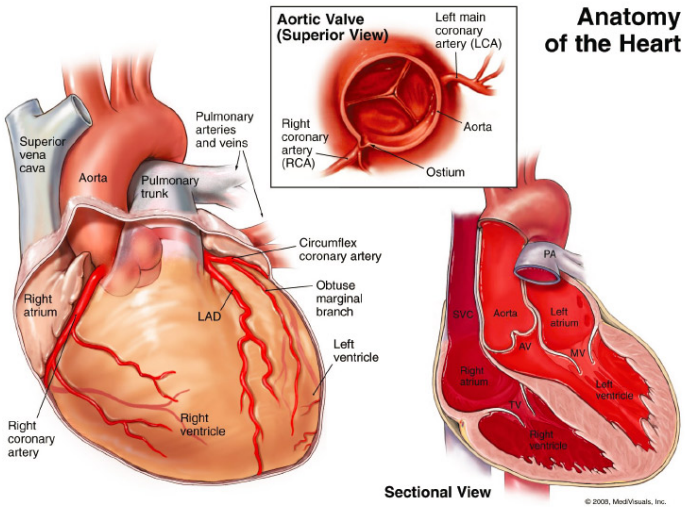

Figure 1.3 Anatomy of a normal heart detailing the location of the coronary arteries. [14]

Total coronary blood flow (Q_{COR} or CBF) is said to be about 4% of the CO and predominantly occurs during diastole [15]. This time dependent flow is related to the interaction of the systemic ventricle and myocardium with the coronary vessels [13]. During systole, the ventricle contracts and increases the intramyocardial tissue pressure [16], squeezing the coronary vessels and increasing their resistance to arterial coronary blood flow (CBF). Additionally, the forward-moving cardiac output opens the aortic valve and the valve leaflets form a barrier between the coronary ostia and the flow (Figure 1.4).

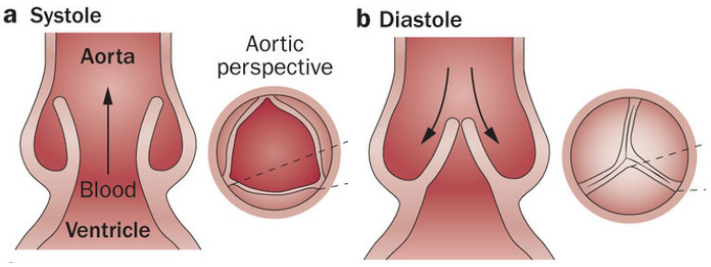

Figure 1.4 The aortic valve leaflet position during (A) systole and (B) diastole. Arrows show blood flow direction [17]**.**

As seen in Figure 1.4, it is during diastole that the aortic sinuses fill and the coronary arteries receive blood. When the aortic valve closes, it is the start of ventricular isovolumetric relaxation and diastole. Here the coronary vessels are least subjected to the intramyocardial pressure from ventricular movement and have the greatest coronary perfusion pressure (CPP): the difference between diastolic aortic pressure and atrial pressure. And so, this is where CBF is at its maximum [18]. Then as the diastolic aortic pressure decreases through the end of the cardiac cycle, the CPP decreases and CBF

responds similarly. This agrees with the echocardiograms (echos) of coronary flow velocities seen in Figure 1.5, where the majority of flow is during diastole.

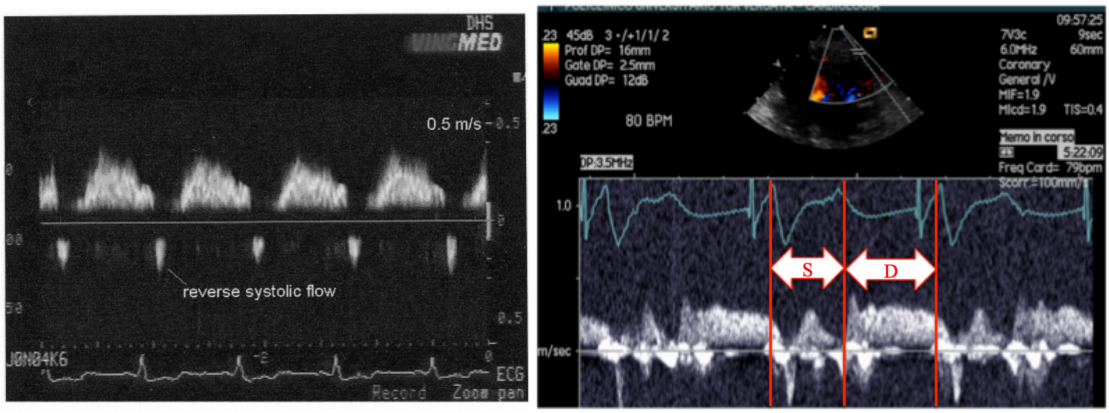

Figure 1.5 Echos of coronary flow of the left anterior descending coronary artery for a (Left) post-aortic-valve replacement patient [19] **and (Right) a normal heart** [20]**. S and D represent systole and diastole, respectively.**

In Figure 1.5, the differences between flow in systole versus diastole are quite distinct for both images. The image on the left is from the Left Anterior Descending artery for a patient who had undergone aortic valve replacement surgery, while the image on the right is from the same artery of a healthy human's heart. It is apparent that the heart receives blood, and thus oxygen, during its relaxed stage of diastole – the supply. It is also clear that during systole, when the heart is exerting itself and in need of energy, it is not receiving as much flow – the demand. This supply-demand relationship can be further understood by the Myocardial Oxygen Supply-Demand Balance (MOB) [18].

The MOB dictates the coronary vasomotor tone's response. This results in vasodilation or vasoconstriction of the coronary vessels to allow for increased or decreased CBF, respectively [21]. The MOB relates the ratio of the amount of CBF the heart needs versus the amount of CBF supplied. Factors affecting the supply of oxygen to

the heart include heart rate (HR), CPP, blood oxygen content, and the diameter of the coronary artery [18]. The demand of oxygen is also governed by HR, preload and afterload on the ventricle, and myocardial inotropy [18]. Thus, the more forcefully and longer the ventricle must contract in systole, the more it will demand oxygen. Likewise, the longer the ventricle is relaxed in diastole or the more pronounced the diastolic aortic pressure, the greater the supply of oxygen to the myocardium. A quantitative measurement of the MOB is made through the Endocardial Viability Ratio (EVR) [21].

The EVR is the ratio of the Diastolic Pressure Time Index (DPTI) to the Tension Time Index (TTI) [21]. The DPTI is the "product of the coronary perfusion pressure and diastolic time," while the TTI is the "product of systolic pressure and systolic time" [21]. In healthy circumstances, the EVR value is 1 or greater, meaning that the oxygen supply meets or exceeds the demand. However, an EVR below 0.7 typically signifies ischaemic conditions [21], meaning the heart tissue is not properly oxygenated for the amount of work it is performing. In these conditions, the blood flow to the coronary circulation is being obstructed. It is important to note that the rate of myocardial oxygen extraction does not increase as substantially as myocardial oxygen demand [16]. Furthermore, an increase in oxygen supply to overcome a low EVR can only be met by an increase in CBF [15]. And so, any deterrent of coronary blood flow will be to the detriment of the heart. Unfortunately, such a deterrent exists in the Stage 1 physiology.

Coronary Arteries in Norwood Physiology

During Stage 1 procedure, some surgeons prefer to not transplant the fragile coronary arteries to the neo-aorta [22]. Instead, as mentioned above, they perform the DKS procedure [23]. In this method, the native aortic root is anastomosed to the neo-aorta, allowing for blood flow from the RV up through the neo-aorta to descend into the native aorta and perfuse the coronaries. In this configuration, the coronary arteries are allowed to maintain their native origin.

Studies have shown that the size of the coronary arteries and ostia between HLHS patients and those of normal conditions do not differ [24]. However, according to Donnelly et al, Norwood patients are said to have "less [coronary] perfusion and oxygen delivery to the systemic ventricle" [12]. Donnelly further mentioned that the hypoplastic LV might even steal from the RV, which is performing an additional workload as it supports both systemic and pulmonary circulations.

In an *in vivo* study of patients after the Norwood surgery, Charpie et al. found that patients requiring medical intervention for decreased ventricular function correlated with having higher Q_P/Q_S ratios and less systemic oxygen delivery than patients who did not need medical intervention [25]. The choice of mBTS, particularly its size, is used to control the Q_P/Q_S ratio. These results reveal the sensitivity that myocardial function has to the mBTS. These findings have been further expressed in other studies that say, when compared to other Stage 1 shunting options, the mBTS has the more devastating effects

on coronary perfusion [8, 10, 11]. These particular effects of the mBTS are referred to as "shunt steal" of the coronary blood flow [10].

Shunt steal of the CBF occurs when the mBTS, which is an open channel throughout the cardiac cycle, "steals" blood that would typically flow towards the coronary circulation. The diastolic aortic pressure, which would normally help perfuse the coronaries, instead directs the flow towards the pulmonary circulation, which has less resistance than the coronary arteries. The end result is that the coronary arteries do not receive as much blood as they typically would. For a single ventricle performing increased workload, the combination of decreased blood supply (which means decreased oxygen supply) and the potential for the hypoplastic ventricle to steal what blood does go to the coronary circulation, the mBTS presents unfavorable odds for ventricular health.

Arguments have been made in favor of other Stage 1 procedures. These would eliminate the mBTS by shunting to the pulmonary circulation using a different method, thus removing the shunt steal's effect on coronary perfusion [2, 6]. For instance, the Right Ventricle – Pulmonary Artery (RVPA) shunt is said to provide better hemodynamics, less shunt steal, and improves overall survival rate to the 2^{nd} surgery [2], [26]. However, the invasiveness of anatomically altering the only healthy ventricle is of concern for some medical professionals. Thus, it is still useful to research improvements to and develop better understanding of the Stage 1 with mBTS. This research can be performed using multi-scale modeling methods.

Multi-scale Modeling of the Norwood with mBTS

In multi-scale modeling, a 3D model is coupled to a zero-dimensional (0-D) LPN, which provides the model's inlet and outlet boundary conditions [27]. In terms of HLHS, multi-scale modeling has been used to model the Norwood palliation for both general and patient specific cases to study the hemodynamics that cannot be captured *in vivo* [28]. These models incorporate a 3D model of interest (i.e. aortic arch) of the HLHS patient that captures the local hemodynamics of the system. The 0-D LPN governs the model's inlet and outlet boundary conditions. The LPN provides the system-level pressures and blood flow rates of the entire "circulatory network" through its use of resistance (R), inertance (L), and capacitance (compliance) (C) elements to create an impedance of each circulation [27]. Migliavacca et al. explained that the reasoning for integrating the LPN to a 3D model is that "the whole circulatory network [of the Norwood palliation] has to be taken into account for the evaluation of the hemodynamics in the specific region [3D model]." [27]

The multi-scale models for the Norwood hemodynamics have been accomplished using experimental (*in vitro*) mock circulatory systems and computational or numerical (*in silico*) models. As described by Biglino et al., some of the key advantages of these models include their ability to acquire detailed information of the hemodynamics that cannot be captured clinically (*in vivo)*, be a tool for educational purposes and medical device testing, and provide "what-if" scenarios for parametric studies of varying surgical options [29]. In the following studies, the aortic arch of a Norwood patient was coupled to a LPN composed of impedances that represent the upper body, lower body, pulmonary,

and coronary circulations. The first of these is an *in silico* study by Migliavacca et al. who looked into the effects of the various shunt options for the Stage 1 surgery. Schematics of their models are seen in Figure 1.6.

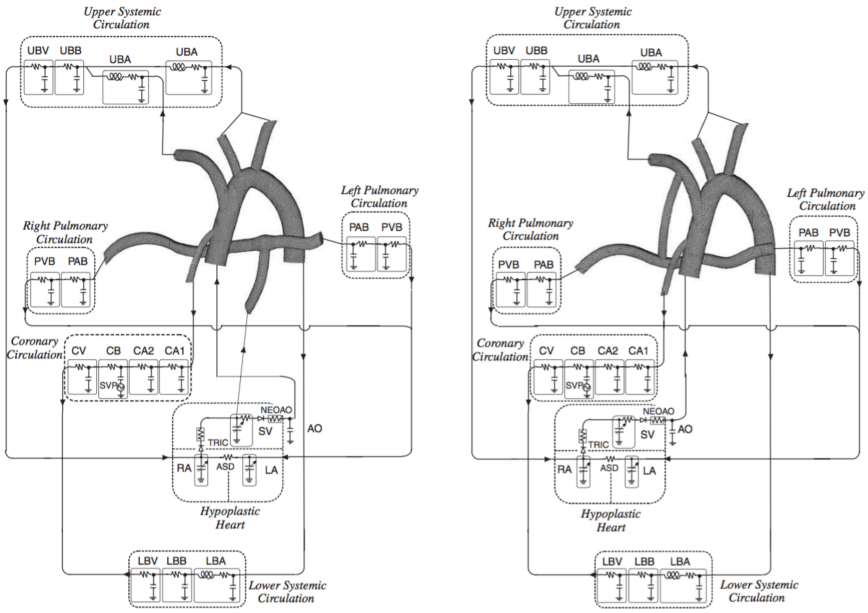

Figure 1.6 *In silico* multi-scale models of the Norwood with RVPA (Left) and mBTS (Right) [27]

In this study, Migliavacca et al. found that the choice of shunt had a large effect on the relationship between pulmonary flow and coronary perfusion. The RVPA shunt, when compared to mBTS, had the greatest CBF because it allowed for a higher diastolic aortic pressure [27], and thus greater CPP. However, the central shunt (CS), which connects from the ascending aorta to PA to provide for systemic to pulmonary flow, lowered the coronary perfusion pressure and flow. It also had more pulmonary flow than the mBTS. This shows the relationship between the systemic-pulmonary shunt's placement and coronary perfusion. It appears that shunts placed in closer proximity to the ascending aorta result in more pulmonary flow and less CBF.

In an *in silico* study that only looked at the mBTS, focus was given to the effects caused by placement and size (inner diameter) of the shunt. Here, Moghadam et al. found that the shunt diameter had a greater effect on coronary oxygen delivery than did the placement (proximal or distal) along the innominate artery [9]. Specifically, a smaller shunt increased the aortic pressure, which allowed for more coronary flow due to a higher CPP. A shunt placed distal along the innominate artery also allowed for optimal coronary oxygen delivery, whereas a proximal placement optimized non-coronary systemic oxygen delivery. For a combined optimization of systemic and coronary oxygen delivery, Moghadam et al. found that a shunt placed between the distal and proximal location with a 3.41 mm diameter was most efficient [9]. These results agreed with Migliavacca et al.'s findings that mBTS size affects the PVR in such a way that blood in the aortic arch during diastole is stolen from the coronaries.

Lagana et al. also looked at the effects of the mBTS compared to the CS with their computational multi-scale model. In this study, the results agreed with Moghadam et al.: the mBTS was better than the CS for coronary perfusion, but increasing mBTS diameter did increase pulmonary flow at the loss of coronary. Further, Lagana et al. found that coronary flow made up 2.98% to 3.83% of the cardiac output when using the mBTS, and that halving the coronary resistance greatly increased the coronary perfusion. This indicates that coronary resistance is a major contributor to determining CBF. Overall, the mBTS was recommended over the CS as the Stage 1 shunt option [11].

In a study focused solely on the mBTS, Corsini et al. used their *in silico* model to see how coarctation (COA), a localized narrowing of the aorta, and mBTS size affected coronary perfusion. A large shunt with severe COA was found to be unfavorable for the coronary perfusion and oxygen delivery. The severe COA caused an increase in the afterload, and resulted in decreased cardiac output. The idea of shunt steal was supported as increased COA severity resulted in an increase Q_P/Q_S and decreased coronary flow. When maintaining constant cerebral perfusion, similar results were obtained [10].

Overall, these *in silico* models come to the same conclusion: the mBTS provides better hemodynamics than the CS, while underperforming compared to the RVPA. When looking only at the mBTS, larger shunt options decreased the diastolic aortic pressure, and so decreased CPP and coronary oxygen delivery. COA in the presence of the mBTS further hinders the coronary performance. These results were performed exclusively using computational methods and rely on the methods chosen to solve the local fluid dynamics of the 3D model – a risk in using *in silico* models. Therefore, the *in vitro* models are useful in their ability to reliably provide the local hemodynamics of the 3D model being studied. Together, the *in vitro* models can be used to verify the results obtained from *in silico* models. Unfortunately, an *in vitro* model of the Norwood palliation that includes the coronary circulation does not exist.

Prior to the work detailed in this thesis, Hang's *in vitro* model for the Stage 1 palliation was limited to providing details about the pulmonary, upper body, and lower body circulations [28]. In his research, Hang validated his MCS against patient-specific

parameters obtained clinically. He then investigated the effects of COA on both the mBTS and RVPA Norwood palliations by introducing a range of COA severities to the model. Five patient-specific 3D models were used in his study to further investigate the effects of morphology. His findings showed that the RVPA does improve the Q_P/Q_S when compared to the mBTS. He also showed that severe COA resulted in more drastic changes to Q_P/Q_S, and that atypical aortic arch morphology was associated with larger ventricle power [28].

In terms of the results on pulmonary to systemic flow, Hang's results agree with those found by the aforementioned *in silico* models. However, the *in vitro* model did not include the coronary circulation. As shown above, coronary perfusion and oxygen delivery are heavily dependent on modifications that affect Q_P/Q_S. This leads to the objectives of the present study.

Research Objectives and Hypothesis

The following are the objectives of this study:

1. Design and integrate a coronary circulation into a previously validated *in vitro* multi-scale model [28]
2. Verify the system's response against a mathematical (analytical) model
3. Validate the *in vitro* coronary blood flow against clinical findings in literature
4. Validate the entire *in vitro* model against clinical data of a HLHS patient
5. Investigate the effects of mBTS size on coronary perfusion

Additionally, the following is hypothesized:

6. The *in vitro* model will illustrate how increased mBTS size negatively affects coronary perfusion

The hypothesis will be accepted in the case where increased shunt size results in decreased coronary blood flow and a connection between the two can be proven. The hypothesis will be rejected in the case where there is no discernable drop in coronary blood flow with increasing shunt size.

In completing these objectives, the *in vitro* model will allow experimentation of the Norwood hemodynamics and morphology with respect to coronary perfusion. In particular, assessing the mBTS's effect will allow detection of whether or not shunt steal of coronary perfusion exists. No experimental findings have been recorded for this phenomenon and doing so would either verify or negate *in silico* results. In the next chapters, focus will be given to the methods taken to create this system, in particular to the coronary circulation.

CHAPTER TWO

IN VITRO CORONARY CIRCULATION MODELING

Early Coronary Blood Flow Models

A major complication of CBF is its interaction with myocardial contraction and relaxation. The upper body, lower body, and pulmonary circulations in *in vitro* LPNs have static impedances whose blood flow and pressure are strictly governed by the fixed impedance values, the upstream aortic pressure, and downstream atrium pressure [28]. This is unlike the coronary circulation, whose impedance must account for myocardial contraction through a dynamic response. This complication was initially addressed by Downey and Kirk's waterfall model [30] and then improved on by Spaan et al.'s intramyocardial pump (IMP) model [31] (Figure 2.1).

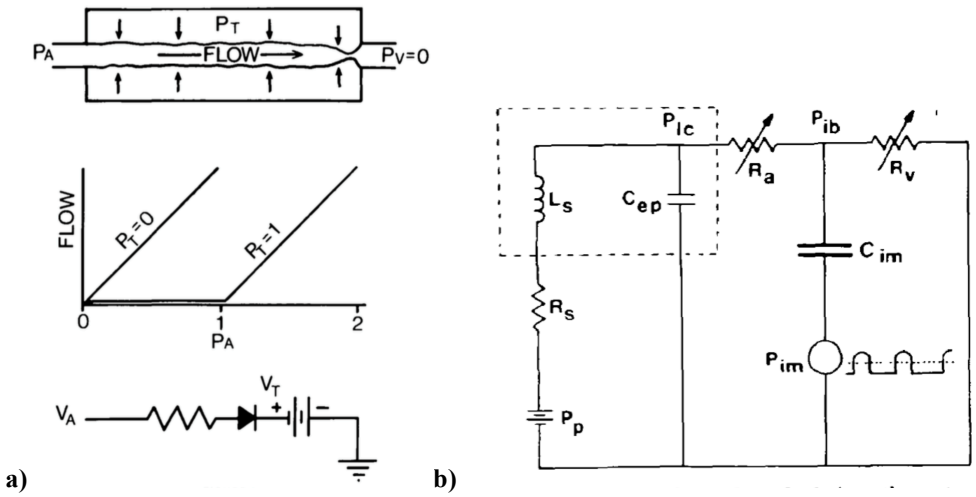

Figure 2.1 (a) Schematic of the waterfall model by Downey and Kirk [32]**: (top) collapsible tube with inflow pressure P_A, outflow pressure P_V, exterior pressure P_T. (middle) flow graph as a function of P_A for two cases of P_T. (bottom) electrical analogue of where V_A is P_A, V_T is P_T, and current is flow. (b) Schematic of the intramyocardial pump model by Spaan et al.** [31]**: intramyocardial tissue pressure P_{im} and capacitance C_{im}, arterial and venous coronary resistances R_a and R_v, intramyocardial blood pressure P_{ib}, perfusion pressure P_p, and left coronary artery pressure P_{lc}. Figures reprinted with permission of original authors.**

The waterfall model (Figure 2.1a) is a "time-varying resistance model" for CBF [31]. Downey and Kirk believed that intramyocardial tissue pressure increases in systole as a result of the cardiac contraction. As the intramyocardial tissue pressure increases during systole, the pressure difference between the tissue and within the coronary vessels results in the vessels collapsing, thus increasing the vessels' resistance [30, 32]. And by the relation that flow is determined by pressure drop across resistance, the arterial pressure drives the coronary flow over coronary resistance towards the venous pressure. The variations in the flow are strictly determined by the variations in the coronary resistance, which is governed by intramyocardial tissue pressure.

To simulate this idea, Downey and Kirk's model (top of Figure 2.1a) is composed of an arterial pressure (P_a) and venous pressure (P_v), whose difference drives the flow through the coronary vessel (i.e., a tube). The outer pressure (P_T) represents the intramyocardial tissue pressure, which increases and decreases during systole and diastole, respectively. When P_T exceeds the pressure within the tube, the tube will increasingly collapse, mimicking an increased coronary vessel resistance during ventricular contraction of systole [32]. This method is able to capture phasic differences in arterial coronary flow: zero-flow during systole when P_T is high and increased flow in diastole when P_T is low. However, it does not account for the systolic flow reversal seen *in vivo* or for the venous coronary flow which is predominately during systole [31, 33]. This led Spaan et al. to develop their IMP model.

To account for accurate arterial and venous coronary flow, the IMP model built on the ideas of the time-dependent diode (resistance) model of Downey and Kirk. For the IMP model, Spaan et al. implemented a volume pumping mechanism by incorporating a capacitor connected to a time-dependent pressure (Figure 2.1b) [31]. They reasoned that in addition to varying resistances to account for autoregulation, coronary vessels also have their own capacitance. When combined with the time-varying intramyocardial tissue pressure, the capacitance of the vessels helps regulate the differences between arterial and venous coronary blood flow through blood volume changes [31]. The volume changes are then directed upstream or downstream depending on the resistance of the arterial and venous coronary beds.

From the schematic in Figure 2.1b, the time-varying intramyocardial pressure (P_{im}) is translated across the intramyocardial capacitor (C_{im}) to the "intramyocardial blood compartment" pressure (P_{ib}) [31]. This results in variations of the P_{ib} pressure, resulting in a higher pressure in systole relative to diastole. With this change in pressure there is also a change in blood volume stored at the capacitor, C_{im}. The direction (flow) and amount of the blood volume is then determined by the arterial and venous coronary resistances (R_a and R_V, respectively), and by the P_{ib} pressure relative to its up and downstream pressures.

In systole, arterial flow is low and may even be retrograde when P_{ib} exceeds the upstream pressure. Further, in systole, the venous coronary flow is driven forward across the venous resistance (R_v) because of the high P_{ib}, mimicking cardiac contraction

squeezing venous blood out of the coronary circulation. In diastole, P_{ib} is lower and is not as influenced by P_{im}. This allows for flow across the arterial resistor to then be stored within C_{im}. Therefore, as that arterial flow moves into the capacitor during diastole and P_{ib} is low, the venous flow is at its minimum. An illustration of this model's arterial coronary flow relative to the systemic LV pressure can be seen in Figure 2.2.

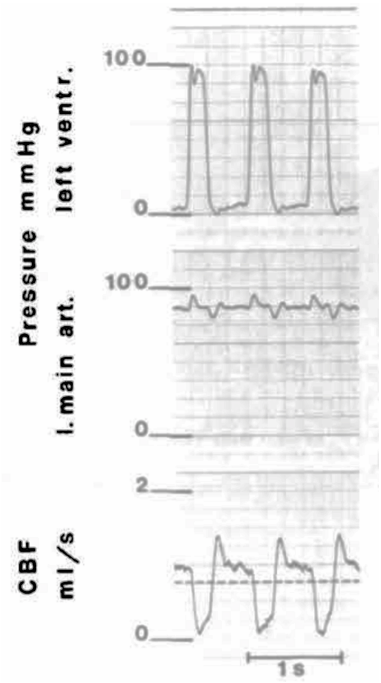

Figure 2.2 Results from the IMP model and reprinted with permission by Spaan et al. Top is left ventricle pressure, middle is coronary artery pressure, and bottom is coronary artery flow. [31]

The waterfall and IMP models were both groundbreaking in their ability to create physiological portrayals of coronary blood flow and pressure. Since these models were proposed, both *in silico* and *in vitro* models have been attempted based on their ideas. The following *in vitro* models are not specifically Norwood models, but were investigated to ensure that the most accurate method was chosen for the Stage 1 MCS.

In Vitro Coronary Blood Flow Models

In recent years, limited accounts of experimental modeling of coronary blood flow have been attempted [34–37]. Their aims were to create a representative circulation that could model varying physiological conditions. An early attempt was by Geven et al. who created a model for an adult human under normal and hyperemic conditions. Their goal was to help validate the then newly developed "clinical diagnostic techniques" that were used to capture coronary flows and pressures [34]. The model can be seen in Figure 2.3.

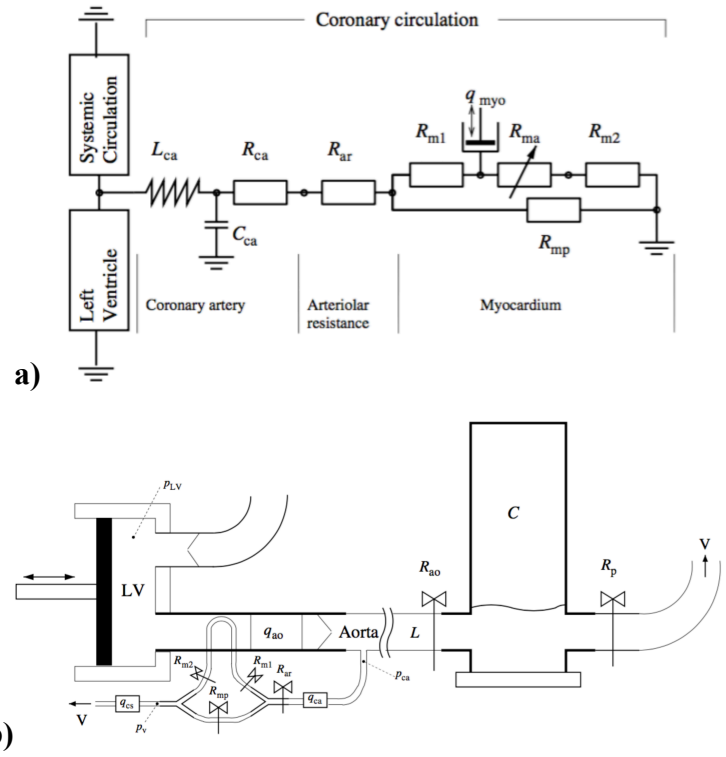

Figure 2.3 Schematics of the (a) LPN coronary model and (b) *in vitro* setup by Geven et al. [34]

In this model, Geven et al. modeled three components of the cardiovascular system: the systemic LV and aorta, the systemic circulation, and the coronary circulation. The LV is a piston-cylinder mechanism composed of an incoming venous flow and outgoing

arterial flow to provide the inlet condition to the aorta: the aortic pressure and flow waveforms [34]. The determinant of these waveforms is the systemic circulation, which is made of a single compliance and a proximal and distal resistance. As fluid moves through the aorta, it is allowed to pass into the coronary circulation.

Referencing Figure 2.3a, the "coronary artery" component of this circulation is modeled with "physiological dimensions and capacitance" using a polyurethane tube. The arterial resistance, R_{ar}, and all subsequent resistances (except R_{ma}) are made using "manually adjustable clamps". Similar to the waterfall model by Downey and Kirk, a change in myocardial resistance due to myocardial contraction is accounted for by the q_{myo} and R_{ma} components of Figure 2.3a. In Figure 2.3b, a collapsible tube is shown to pass through the LV chamber so that the inner LV pressure can physically manipulate the resistance of the collapsible tube at this point in the circulation [34]. The authors refer to their work as mimicking Downey and Kirk, however the collapsible tube provides it's own compliance, which is similar to Spaan et al.'s IMP model. This is shown in Geven et al.'s results (Figure 2.4 below) where retrograde systolic CBF is achieved.

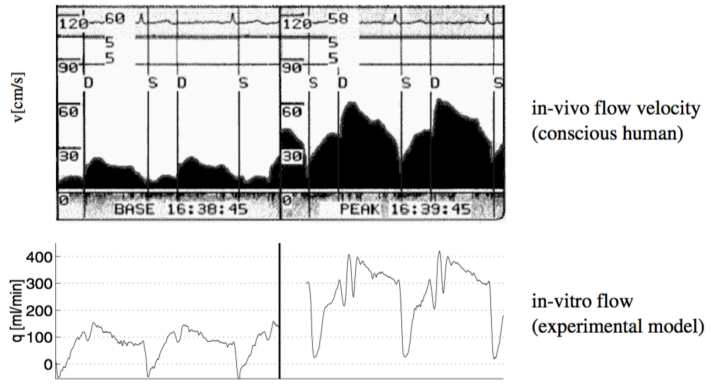

Figure 2.4 Clinical (top) and *in vitro* (bottom) coronary artery flow for normal (left) and hyperemic (right) conditions [34]

The results of Geven et al.'s experiment for normal and hyperemic conditions show distinct differences in systolic versus diastolic flow, while even accounting for retrograde flow during systole. Further, the results qualitatively agree with the *in vivo* reference. However, this model is limited in that it lumps the entire systemic circulation into one impedance element, which does not allow for the individual effects on specific systemic branches to be described. Additionally, while the coronary circulation appears accurate, passing a tube through the LV chamber would present a problem with Hang's *in vitro* setup [28]. Hang used a ventricular assist device (VAD) to provide the aortic pressure and flow waveforms, and this device's structure would not allow for a coronary tube to be passed through it. Therefore, Geven et al.'s exact method would not work for implementation into Hang's MCS.

Pantalos et al. developed a 0-D MCS for pediatric cardiovascular systems [35]. Their bench-top model allowed for various setups to help test different medical instruments such as an intraaortic balloon pump or VADs. Their system, seen in Figure 2.4, comprises both the systemic and pulmonary circulations. The coronary circulation is one single tube running through a "dynamic resistor" [35]. Unlike Geven et al. and Spaan et al., it does not account for compliance of the coronaries. The coronary flow is strictly controlled by the variation in the resistor. Additionally, this model does not account for venous coronary flow, although whether or not this was important to their setup is unknown.

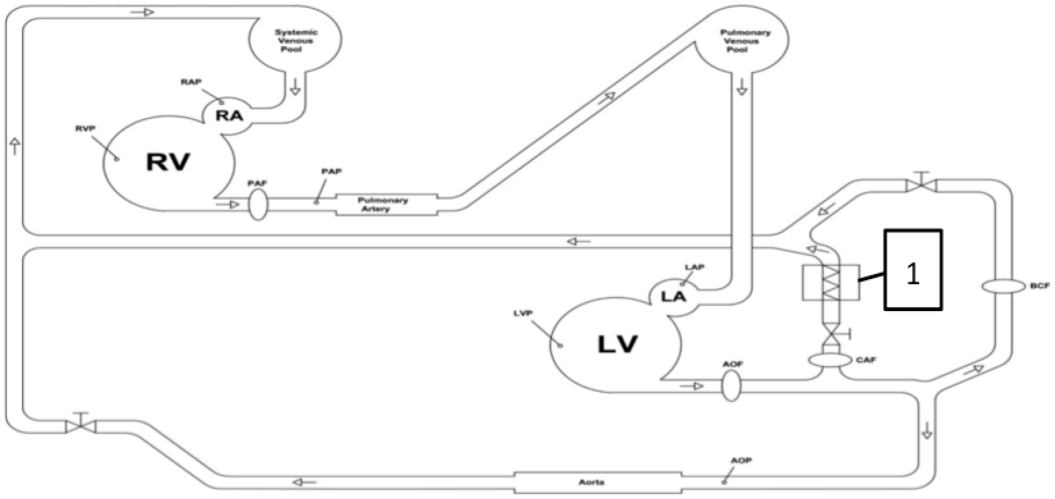

Figure 2.4 Schematic of the experimental pediatric cardiovascular model with the (1) dynamic coronary flow resistor by Pantalos et al. [35]

Looking at the results of Pantalos et al.'s study, clinical validation of their system was only given to ventricle pressure and aortic flow and pressure [35]. The coronary flow was not validated against any *in vivo* measurements. Initially, the model was used in a normal setup, like the one seen in Figure 2.4. Then they modified the system to model the cardiovascular system's response to different medical devices. The literature does not reveal whether the dynamic resistor was able to accurately capture a physiological flow in the coronary circulation, especially when the results reveal such variability between setups (Figure 2.5). Thus, this approach for coronary modeling was discarded.

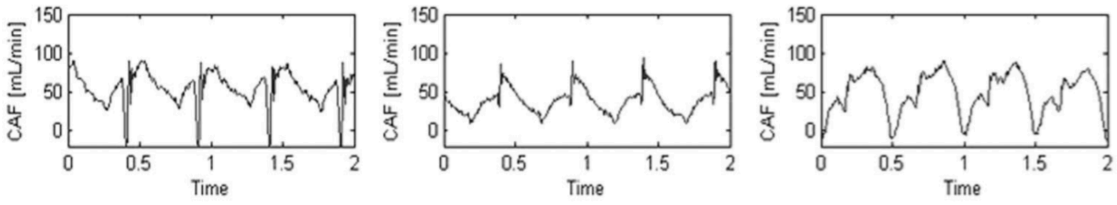

Figure 2.5 Coronary artery flow for (Left) normal, (Middle) LV failure, and (Right) intraaortic balloon pump models [35]

In the same year, Gaillard et al. reported their work on modeling the effects of aortic valve stenosis on the coronary circulation [36]. The model (Figure 2.6) is very similar to that presented by Geven et al [34]. The system is composed of three branches: the ventricle, systemic "aortic flow model", and the coronary circulation. The coronary circulation differs from Geven et al.'s in that it does not pass a collapsible tube through the ventricle's chamber. Instead, a tube is connected from that chamber and is passed to another chamber. The resistor R_{LV} is used to adjust the LV chamber pressure felt in the "Sim" chamber [36]. This chamber has a collapsible tube passing through it so that during systole, the variations in pressure have an effect on the resistance of the flow passing through that area. Further, compliance of the collapsible tube allows for volume changing features to be applied, like those proposed by Spaan et al.'s IMP model [31].

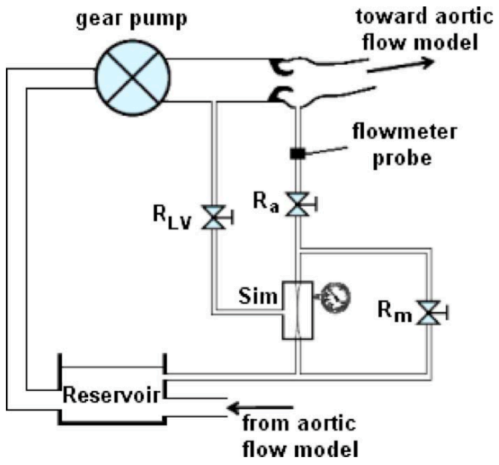

Figure 2.6 Schematic of *in vitro* setup by Gaillard et al. [36]

Unlike Pantalos et al., Gaillard et al. gave attention to the *in vivo* validation of his experiment's results. They used clinical echo measurements from the left anterior descending coronary artery under various levels of aortic valve stenosis to compare

against their results [36]. They found that their waveform of arterial coronary flow was both accurate in shape and magnitude. This clinical validation method is important in determining whether the model is accurate, especially if the parameters of the system are going to be extrapolated beyond the comparable results. And while the model appears to present a reliable results, the method of how they adjusted the R_{LV} is unclear. However, while passing a connecting tube to a VAD is unfeasible for the Hang MCS, the idea of bringing the ventricular pressure to the coronary model was noteworthy.

A final *in vitro* model studied was by Calderan et al. [37]. The purpose of their work was to develop a systemic model that could simulate the effects of "transcatheter aortic valve implantation (TAVI)" [37] on coronary flow. Their entire system was composed of a LV and aorta branch, a systemic impedance to help control the aortic waveforms, and the coronary circulation. The coronary branch was modeled as the simplified LPN seen in Figure 2.7a. It is composed of a proximal static resistance, compliance, and a distal time-varying resistor (R_{ma}) [37].

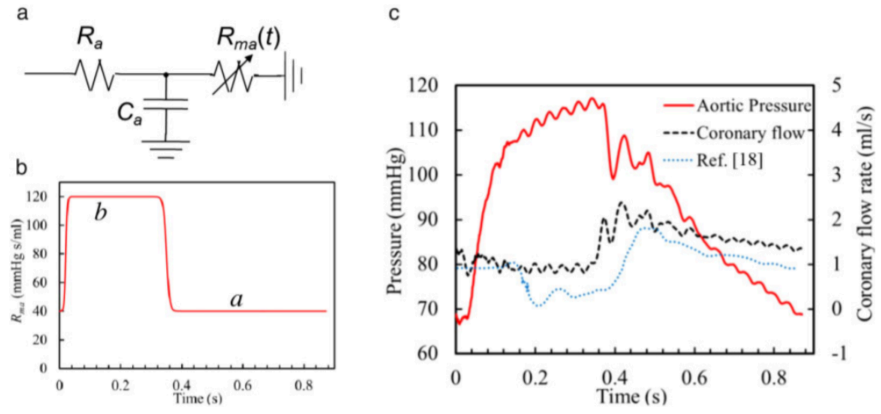

Figure 2.7 Calderan et al.'s (a) coronary LPN, (b) $R_{ma}(t)$ resistance graph for one cardiac cycle, and (c) experimental results of coronary flow and aortic pressure, and *in vivo* coronary flow [37]

The time-varying resistor in Figure 2.7 was achieved using a "stepper motor" connected to an "adjustable stopcock valve" [37]. The amount the valve was closed, the amount of resistance to coronary flow, depended on the signal of R_{ma}, which had a higher value during systole than in diastole (Figure 2.7b) to mimic cardiac contraction impeding the flow. The signal was sent to the stepper motor by a LabView system. Higher magnitudes of resistance correlated with the stepper motor closing the valve more [37].

The coronary flow based on this time-varying resistance model can be seen in Figure 2.7c. As shown, it is in comparable qualitative agreement with the provided clinical reference, however slight amplitude differences are apparent. Further, this model was said to measure the coronary flow distal to R_{ma} [37]. This means that attention was not given to the proximal flow conditions, which may or may not have been physiological. Since the study was to see the effect the TAVI had on coronary flow, the unknown area between the TAVI and measured coronary flow could have had non-physiological features that could interfere with the results. Additionally, this model did not account for a relation of intramyocardial tissue pressure and coronary vessel compliance in the way that Spaan et al. proposed to make distinctions between arterial and venous flow [31]. However, the control of the resistance using LabView is noteworthy considering the same program is used in Hang's setup [28].

Overall these models provide helpful insight into the methods used to capture physiological coronary flow waveforms. Considering these experimental techniques,

attention was then given to the LPN that would be used as the blueprint for the *in vitro* system.

Selecting the Coronary Circulation LPN

When determining the framework of the LPN, it was important to consider the implications of the experimental model used in relation to other Norwood *in silico* models. A model based on a LPN that is very different from those *in silico* versions might not provide the ability for comparable coronary results, in case one system's response was different from another. Therefore, the LPNs from multiple *in silico* models [9–11, 27, 38, 39] of the Stage 1 with mBTS palliation were analyzed with regards to their waveform results, size, and ease of implementation .

The in-depth review of the *in silico* models revealed a familial relationship between the LPNs of the coronary circulations with slight variation through the other branches. Dating from 2005 to 2014, the same coronary LPN was used between the works of Lagana et al., Migliavacca et al., Bove et al., Hsia et al, Moghadam et al., and Corsini et al. [9–11, 27, 38, 39]. Lagana et al. was the first to depict the coronary model in a Norwood model [11]. They built their coronary LPN based on the descriptions by Mantero et al. [13], whose adult-human mathematical model followed the ideas of Spaan et al.'s IMP model [31]. A schematic of the coronary LPN used by these Norwood *in silico* works is shown in Figure 2.8.

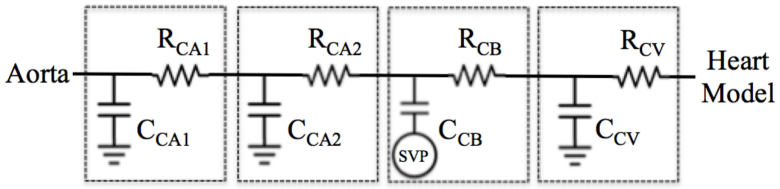

Figure 2.8 Schematic of the LPN used in multiple *in silico* Norwood models

The "SVP" in Figure 2.8 refers to the single ventricle pressure (SVP). For the Norwood palliation, this would refer to the systemic RV pressure, which is connected at the SVP point from the heart model of their LPN. The compliance C_{CB} connected to the SVP mimics the idea of myocardial contraction, which, according to Mantero et al., is felt more in the distal endocardial vessels than the proximal epicardial vessels [13]. Thus, the SVP mostly affects the pressure at the CB resistance and compliance junction, and its impact is decreased from the CA2 impedance to the CA1 impedance.

The different impedance elements in Figure 2.8 allow for the distinction between the arterial coronaries (CA1 and CA2) and the venous (CB and CV). Hence, like the IMP model, both arterial and venous blood flow should be distinguishable based on the point that is measured. To provide the boundary condition to the 3D model in the MCS, it is only necessary to create an arterial coronary blood flow and pressure. However, having the ability to distinguish differences in arterial and venous flow may aid in validating the waveforms.

To the author's knowledge, all coronary LPN models for the Norwood palliation are of the same structure. And so, it was determined that the LPN in Figure 2.8 would be the reference for the *in vitro* model. A slight variation from this model was caused by the

values of the resistors and compliances used in the *in silico* models (Table 2.1). Note that the values for each element in the LPN are scaled based on body surface area (BSA) [40]. Each model uses the same elemental values because BSA remained at 0.33 m^2.

Table 2.1 The LPN values used by the *in* silico models [9]–[11], [27], [38], [39]

	CA1	CA2	CB	CV
Resistance (R) [mmHg.s/mL]	10.6739	10.6739	21.3477	10.6739
Compliance (C) [mL/mmHg]	1.94351×10^{-3}	5.18269×10^{-3}	7.77404×10^{-3}	0.5×10^{-4}

Referring to Table 2.1, relative to the R and C values used for the other systemic and pulmonary circulations, the compliance values are magnitudes smaller and the resistances are very large. In particular, the CV compliance is a magnitude smaller than the three proximal to it. For experimental modeling feasibility, C_{CV} was discarded and the resistance, R_{CV}, which was not negligible, was lumped into R_{CB}. The final LPN and values used for the *in vitro* model are seen in Figure 2.9 and Table 2.2.

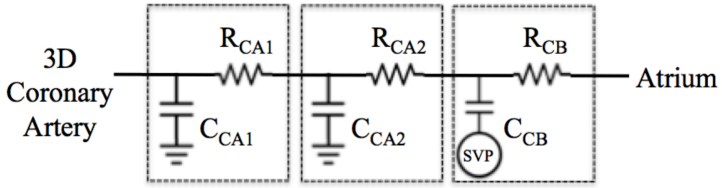

Figure 2.9 The coronary LPN used for the *in vitro* model

Table 2.2 The LPN values for the LPN seen in Figure 2.9

	CA1	CA2	CB
Resistance (R) [mmHg.s/mL]	10.6739	10.6739	32.0216
Compliance (C) [mL/mmHg]	1.94351×10^{-4}	5.18269×10^{-4}	7.77404×10^{-3}

The following section details the experimental implementation and reasoning for discarding C_{CV}. Along with C_{CV} being eliminated, the compliances C_{CA1} and C_{CA2} were reduced in size. A purely mathematical model, created for verification purposes, did not couple a 3D model to the LPN. And so, there were slight differences in how the coronary system responded. Reducing these compliance values achieved a physiological flow waveform, details of which are discussed in the next chapter.

Creating the In Vitro Coronary Circulation

The methods chosen for creating the physical realization of the LPN were based on those used by Vukicevic et al. [41] and Hang [28]. Tubing was used to connect the inflow and outflow ports of the 3D model to the *in vitro* LPN. The amount of tubing was minimized to reduce any effects of inertance and unintentional resistance. To set the resistance, pinch needle valves were used, which cause a change in flow for a give pressure drop based on Equation 2.1

$$R = \Delta P / Q \tag{2.1}$$

Here, Q is the flow rate through the valve and ΔP is the fluid pressure drop across the valve. Additionally, the compliance of an impedance element is based on Equation 2.2.

$$C = \Delta V / \Delta P \tag{2.2}$$

For this fluid system, the effects of C can be described by the change of volume (ΔV) of fluid in the compliant element for a change in fluid pressure (ΔP) [41]. This is created using air chambers that trap a pocket of air [41] coupled to the fluid system which applies

the pressure that compresses the air. For setup purposes, the volume of air is calculated as $V=C*P_{abs}$, where P_{abs} is the mean absolute pressure of the air at that compliance element.

The first two compliances (C_{CA1} and C_{CA2}) were made using 10 mL syringes. Based on Equation 2.2, the volume of air calculated for the C_{CV} value was less than what could be reliably measured. It was assumed that the compliance of the tubing was enough to implement this feature. On the other hand, the compliance at C_{CB} presented its own complication since it is coupled to the SVP

The aim of the *in vitro* coronary model was to mimic the LPN as closely as possible. Methods such as Geven et al.'s [34], where the coronary tubing was passed through the LV chamber, were used as reference in designing the final model but not exactly replicated. Geven et al.'s methods presented a three-dimensional effect of SVP on the *in vitro* coronary LPN. Since this part of the system is supposed to be 0-D, the coronary tubing needed to be affected by SVP at a specific point. This was achieved with the C_{CB}-SVP coupling chamber (CC) apparatus (Figure 2.10).

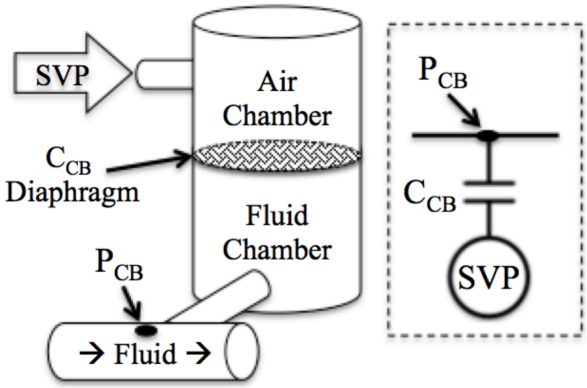

Figure 2.10 Schematic of the experimental C_{CB}-SVP coupling chamber (Left) and LPN (Right)

In Figure 2.10, a pneumatic SVP signal is applied to the air-filled side of the CC. This signal is then translated across a diaphragm to the fluid chamber of the CC. This chamber is connected to the main coronary tubing at the CB pressure point (P_{CB}). By minimizing the SVP contact to a point within the main coronary tubing, control of P_{CB} for tuning purposes is maintained. Throughout the cardiac cycle, as the SVP is applied, the diaphragm will appropriately flex to affect P_{CB} accordingly. The flex of the diaphragm accounts for volume displacement, allowing for the variation in arterial and venous flow as described by Spaan et al. The final *in vitro* coronary circulation is seen in Figure 2.11.

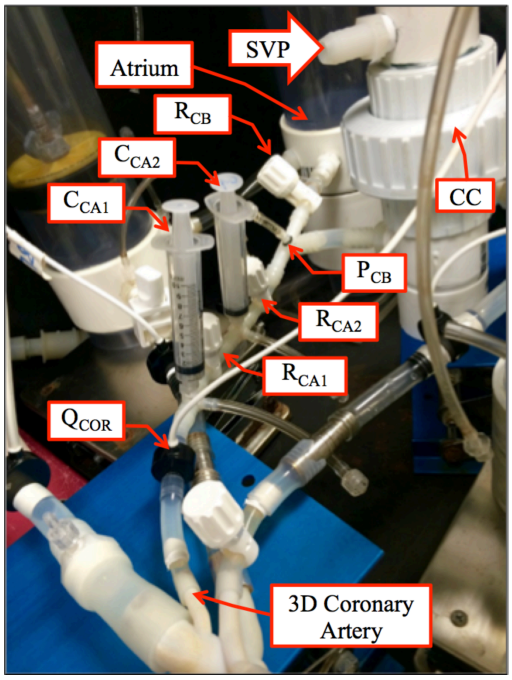

Figure 2.11 The *in vitro* coronary circulation

The CC was made of PVC pipe and fittings. The diaphragm's material, a silicone rubber, was chosen with respect to how it interacted with the fluid chamber. Thus, the diaphragm's compliance was C_{CB}. Furthermore, a 3-way valve (Model: 225B-111CAAA,

MAC Valve, Dundee, MI, USA) was used to connect an incoming compressed air line and vacuum line with the output going to the SVP. Pressure regulators were used to control the magnitude of the incoming pressure and vacuum pressure. The ratio of time for compressed air to vacuum was sent to the 3-way valve as a computer generated signal from the data acquisition/control system (DAQ) and LabVIEW (USB 6211, LabVIEW 8.6; National Instruments, Austin, TX). A schematic of this setup is shown in Figure 2.12.

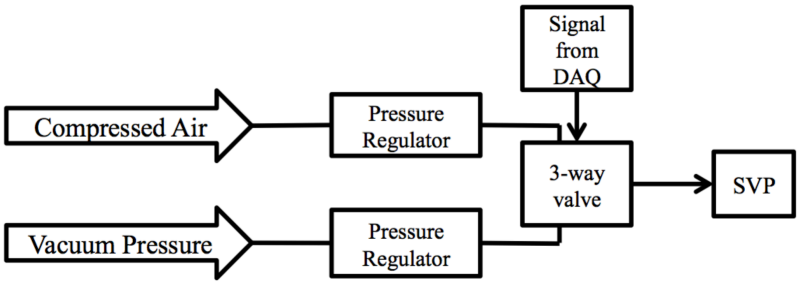

Figure 2.12 Schematic of the setup used to create the pneumatic SVP signal

Coronary flow (Q_{COR}) measurements, using a 5.1mm diameter electromagnetic flow probe (Model: EP616-STD-PV8-501, Carolina Medical Electronics, King, NC), were taken between the 3D model and the first impedance to ensure the proper arterial boundary condition was met. Pressure measurements were taken at the syringe-tubing unions (P_{CA1} and P_{CA2}) and at the CC-tubing union (P_{CB}). Wall taps were connected to pressure transducers (DTXplus, BD Medical Systems, Sandy, UT). All signals were acquired using the DAQ at 160 Hz. Full details of system equipment, setup, and tuning can be found in Appendix A.

CHAPTER THREE

THE *IN VITRO* MOCK CIRCULATORY SYSTEM

The In Vitro Model

A LPN of the entire cardiovascular system, with the addition of the coronary circulation, was created based on the structure of Hang's LPN [28]. The MCS features the LPN coupled to a 3D model (test section) of the reconstructed aortic arch. A schematic of the MCS is shown in Figure 3.1 (Left) and a photograph of the MCS is shown in Figure 3.2 (Right). A VAD is used as a hydraulic pump whose output passes through a proximal compliance (C_{prox}) to provide the input aortic flow (Q_{AO}) and pressure (P_{AO}) to the test section. From the test section, the fluid passes into the systemic branches: upper body (UB), lower body (LB), and coronary (COR), and a pulmonary/mBTS (mBTS) branch. All circulations return the fluid into the atrium (Atr) that then reconnects to the VAD.

To run experiments with this system, the first step was to tune the *in vitro* LPN's resistance and compliance. These impedance values were determined by either an analytical model or clinical data. Once tune, the VAD and proximal compliance (C_{PROX}) were adjusted to create the appropriate input aortic pressure waveform. With the impedance downstream of the test section set, once the correct waveform was created, then the resulting flows and pressures were measured.

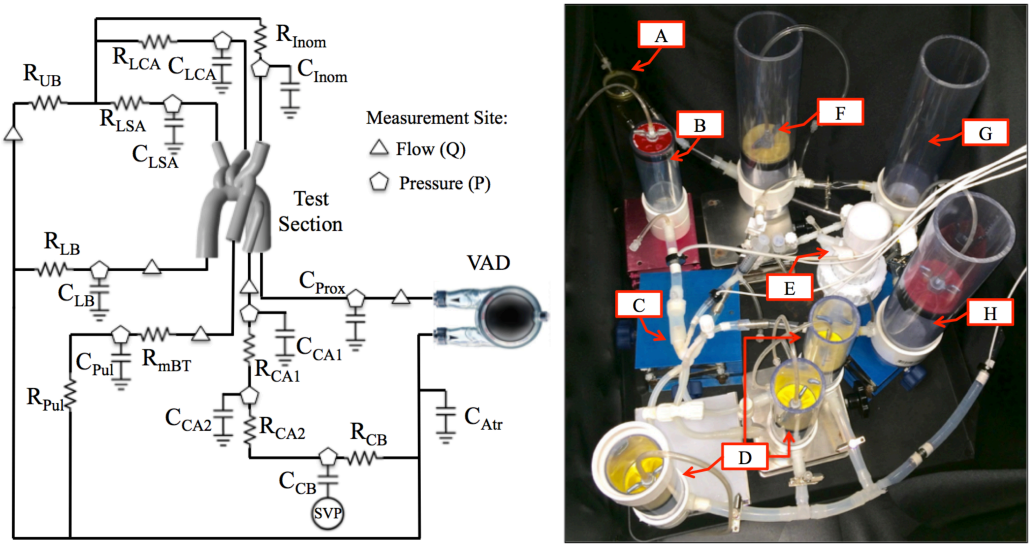

Figure 3.1 The MCS schematic (Left) and *in vitro* MCS (Right): (A) VAD, (B) Proximal Aortic Compliance, (C) Test Section, (D) Upper Body, (E) CC and Coronary, (F) Lower Body, (G) Atrium, (H) mBTS and Pulmonary. Points of flow (Q) and pressure (P) measurements.

Similar to the coronary *in vitro* model, air chambers and pinch needle valves were used as compliance and resistance in the other systemic and pulmonary branches. The atrium was assumed to have infinite compliance and was left as an open reservoir. All flow measurements (referenced markers in Figure 3.1) were taken using electromagnetic flow probes (EP600 series, Carolina Medical Electronics, King, NC) controlled by an analog flow meter (FM501, Carolina Medical Electronics, King, NC). Pressure measurements were taken at pressure wall taps (referenced markers in Figure 3.1). The signal was acquired using pressure transducers (DTXplus, BD Medical Systems, Sandy, UT) and passed through a bridge amplifier (Model 2100, Measurements Group Inc., Raleigh, NC). Both flow and pressure signals were measured and recorded using a data acquisition system (DAQ) and LabVIEW (USB6211, LabVIEW 8.6; National Instruments, Austin, TX). Compressed air and vacuum were used to control the VAD,

similar to the system that created the coronary system's SVP. Both systems used the same air and vacuum lines but were independently controlled for systolic time ratio.

The Methods to Verify

In order to verify that the *in vitro* MCS was setup correctly, a purely mathematical model of the LPN (Appendix B) of Figure 3.1 was created. This analytical model was set up for a baseline case using parameter values from Corsini et al.'s LPN [10], whose values were derived from pre-Glenn patients' catheterization data. Then, with a prescribed aortic flow and pressure input, the analytical model's LPN provided the flow and pressure measurements for the subsequent circulations. These were used for setting the resistance and compliance of the MCS, controlling the VAD to achieve the desired aortic waveforms, and controlling the air pressure of the SVP. A saline solution (30 cc salt per gallon of water) was used as the system's fluid. The heart rate (HR) was 120 beats per minute (bpm), which correlated to a 0.5 second cardiac cycle.

A generalized HLHS post-Norwood 3D model used by Corsini et al. [10] was provided. The model (Figure 3.2) has a 3.5 mm inner diameter mBTS connected at the innominate artery, and a representative coronary artery (2 mm inner diameter) at the site of the DKS anastomosis. The test section was printed in 3D and used for the verification study only. The 3D model was based on a BSA of 0.33 m^2. Based on the scaling laws defined by Pennati and Fumero [40], the coronary LPN values from Table 2.2 did not change. A full set of LPN values and system tuning details are found in Appendices A and B.

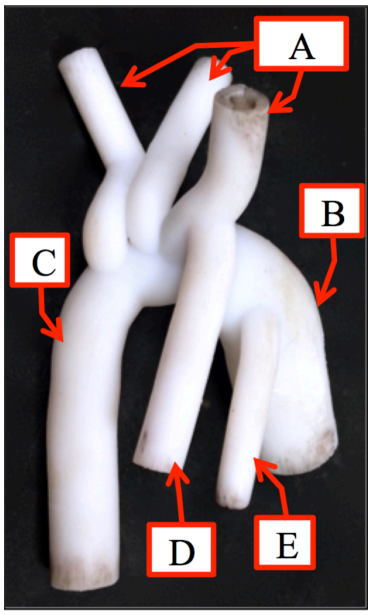

Figure 3.2 The 3D-printed test section for the verification study: (A) *Left to Right*: Left Subclavian (LSA), Left Carotid (LCA), Innominate (Inom), (B) Ascending Aorta (AO), (C) Descending Aorta to Lower Body (LB), (D) mBTS, (E) Coronary (COR)

Verification Results

The system was set for the flow and pressures from the analytical model (Appendix B). The experimental (or MCS) mean pressure (P) [mmHg], mean flow (Q) [Lpm], and resistance (R) [WU = mmHg/Lpm] results can be seen alongside the analytical values in Table 3.1. All MCS results were averaged over 10 cardiac cycles worth of data to ensure stable results. A t-test at 95% confidence was performed to compare mean MCS and analytical results. Methods for statistical analysis and uncertainty are found in Appendix C. The resistance values were calculated using Equations 3.1-3.5. MCS and analytical waveform relationship was quantified through the coefficient of determination (R^2) and a range-normalized Root-Mean-Square Error (σ) (Equation 3.6). Full results are in Appendix D.

Table 3.1 Mean flow, mean pressure, and resistance results for the verification study. MCS values = mean ± uncertainty

Flow [Lpm]	**Analytical**	**MCS**
Cardiac Output (Q_{AO})	1.82	1.82 ± 0.01
Upper Body (Q_{UB})	0.38	0.38 ± 0.01
Lower Body (Q_{LB})	0.40	0.40 ± 0.01
Pulmonary (Q_{mBTS})	0.98	0.98 ± 0.01
Coronary (Q_{COR})	0.056	0.056 ± 0.002
Pressure [mm Hg]	**Analytical**	**MCS**
Ascending Aorta (P_{AO})	60.11	60.37 ± 0.30
Pulmonary (P_{Pul})	11.06	11.05 ± 0.06
Lower Body (P_{LB})	56.71	57.56 ± 0.29
Coronary CA1 (P_{CA1})	53.61	57.51 ± 0.28
Coronary CA2 (P_{CA2})	43.71	43.89 ± 0.22
Coronary CB (P_{CB})	33.80	33.61 ± 0.18
Resistance [WU]	**Analytical**	**MCS**
Upper Body (UBSVR)	148	150 ± 4
Lower Body (LBSVR)	139	140 ± 3
mBTS (R_{mBTS})	50	50 ± 1
Pulmonary (R_{pul})	7	7 ± 0.1
Total Coronary (R_{TC})	1000	1005 ± 35

$$UBSVR = (P_{AO} - P_{Atr})/Q_{UB} \tag{3.1}$$

$$LBSVR = (P_{AO} - P_{Atr})/Q_{LB} \tag{3.2}$$

$$R_{mBTS} = (P_{AO} - P_{Pul})/Q_{mBTS} \tag{3.3}$$

$$R_{Pul} = (P_{Pul} - P_{Atr})/Q_{mBTS} \tag{3.4}$$

$$R_{TC} = (P_{AO} - P_{Atr})/Q_{COR} \tag{3.5}$$

$$\sigma = \frac{\sqrt{\frac{1}{N}\sum_{i=1}^{N}(y_i - y_{ci})^2}}{y_{max} - y_{min}} * 100\% \quad (3.6)$$

Table 3.1 shows the experimental (MCS) mean results are in good agreement with the analytical model. A 30 mm circumference flow probe was used to measure Q_{AO}, Q_{UB}, Q_{LB} and Q_{mBTS}. A 15 mm circumference flow probe was used to measure Q_{COR}. The probe sizing and relative magnitude of flow velocities resulted in less uncertainty for the coronary flow, details of which are discussed in Appendix C. The t-test results do not show any significant difference ($p > 0.05$) for the flow measurements.

For pressure, only the pulmonary pressure was found to have no statistical difference ($p=0.25$) between the mean analytical and MCS values. However, P_{AO}, P_{pul}, P_{CA2}, and P_{CB} were encompassed in the uncertainty of MCS results and so the values were deemed acceptable. The largest difference was found at P_{CA1}, with a relative error of less than 8%. This difference may be the result of comparing a purely analytical model whose impedance was not able to capture that of the multi-scale model's 3D test section. Therefore, the results obtained were deemed sufficient. This can be shown further when comparing P_{AO}'s analytical and MCS waveforms (Figure 3.3).

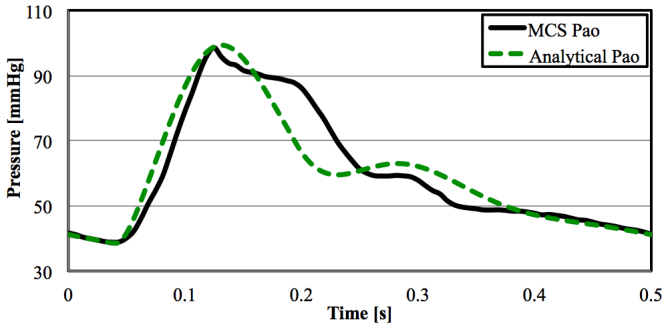

Figure 3.3 Analytical and *in vitro* waveforms of aortic pressure (P_{ao}) (R^2=0.91, σ=8.6%)

The aortic pressures for the analytical and MCS waveforms are highly correlated (R^2=0.91, σ=8.6%). The proximal compliance was calculated to be 0.094 mL/mmHg compared to the analytical value of 0.095 mL/mmHg, and the pulse pressures were within 1% of each other. The P_{AO} is the input boundary condition to the test section and governs the response of the subsequent circulations. As Table 3.1 indicates close agreement with the analytical and MCS values for those subsequent circulations, it can be concluded that the MCS's impedance was appropriately set. Even more so, the addition of the coronary branch did not seem to negatively affect the performance of the other circulations. Those parts of Hang's MCS [28] were replicated. It was then important to verify that the *in vitro* CBF model was acting correctly alongside the rest of the system.

Verification of the Coronary Blood Flow Waveform

The aim in verification is to produce the analytical results using the MCS. However, it is important that these results are consistent with what might be found clinically. While echos of healthy coronary blood flow have been shown, it is important to consider that HLHS patients may present abnormal flow. However, HLHS and congenital heart disease patients' coronary flow reveal the same general characteristics previously described. This can be seen in the following image of the flow velocities in an epicardial coronary artery of a neonate with HLHS and coronary fistulas: pathways from coronary vasculature into the ventricle [33].

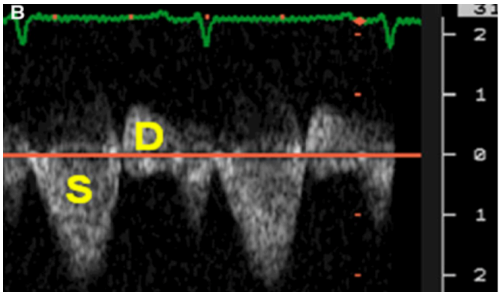

Figure 3.4 Doppler echos of epicardial coronary arteries in HLHS neonate [33]**.**

In Figure 3.4, the "S" and "D" stand for systole and diastole, respectively. It can be seen that the flow is primarily forward (antegrade) toward the heart in diastole. While systole, particularly in this case, the flow is primarily retrograde. Roberson et al. explains that this particularly high systolic retrograde flow may be the result of the fistulas, which aren't always present in HLHS patients [33]. This reveals that CBF characteristics are unique to the patient and measurement site. This is seen when comparing Figure 3.4 to Figure 3.5.

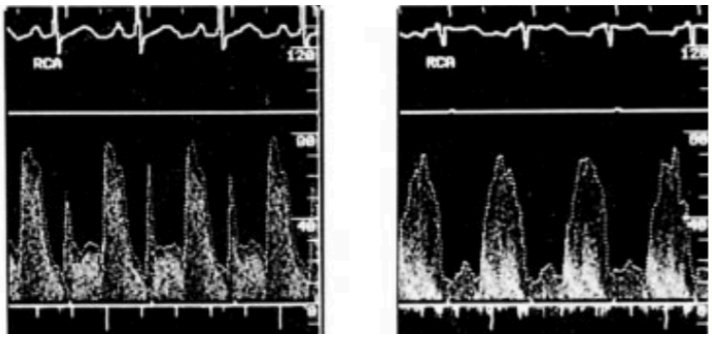

Figure 3.5 Right coronary artery flow velocities for congenital heart disease patients [42]**.**

In Figure 3.5, the right coronary artery flow velocities are both different when compared against each other, and even more so when compared to Figure 3.4. Nonetheless, the same pattern persists. The common characteristics for HLHS patient arterial CBF include low systolic flow, early retrograde systolic flow, dominant diastolic

flow, and peak flow at the beginning of diastole [16, 21, 33]. The goal of the *in vitro* CBF waveform created is to provide a representative arterial coronary boundary condition to the test section. With this in mind, the analytical and *in vitro* waveforms (Figure 3.6) are both in agreement with the coronary flow characteristics, as well as with each other.

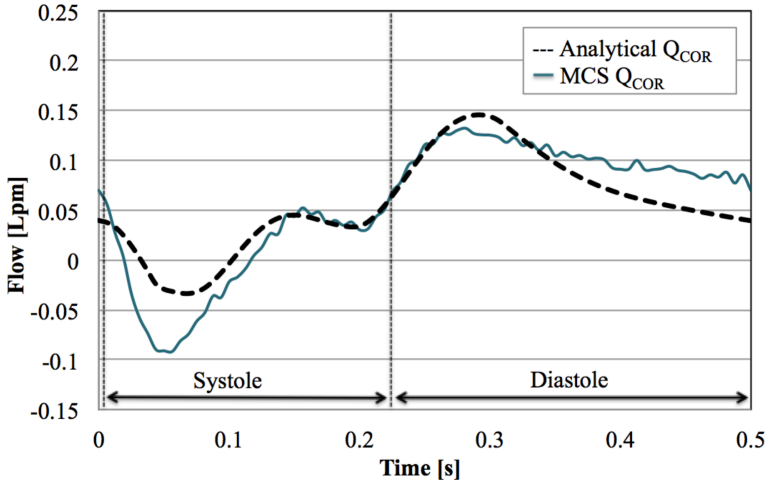

Figure 3.6 Analytical and *in vitro* coronary flow for the verification study (R^2=0.83, σ=14.7%)

The CBF waveforms in Figure 3.6 both show retrograde flow during systole, peak flow at the start of diastole, and a downward-trending flow through the rest of the cardiac cycle. Furthermore, the MCS Q_{COR} clearly indicates a majority of the arterial CBF occurs in diastole. Therefore the shape of Q_{COR} in relation to the cardiac cycle is acceptable as it agrees with literature references for CBF. Additionally, no significant difference (p=0.85) was found between the analytical and MCS mean values, and a correlation between the data was strong (R^2=0.84, σ=14.7%). This indicates an agreement between the analytical coronary model and the *in vitro* coronary model.

From Figure 3.6, deviations in the magnitude of the retrograde systolic flow and slope of the descending diastolic flow do exist between the analytical and MCS Q_{COR}. The

variation may be explained by the difference in pressure at P_{CA1} (Table 3.1), which may indicate a difference in coronary impedance. To further understand the effect of impedance on the CBF waveform and ensure that the C_{CB}-SVP coupling (CC) would respond appropriately to local changes, the following study was performed.

In Vitro Coronary System Verification

The aim of this study was to verify that the *in vitro* coronary system is an accurate model of the LPN from Figure 2.9. The previous section ensured the system provided physiological results that matched a specific analytical case. It was then important to see if the model's coronary hemodynamics would also respond to changes in the coronary system with both accurate and physiological results. This was accomplished by assessing three aspects of the system: the ability to produce arterial (Q_{COR}) and venous (Q_{CV}) coronary flow, the response to changes in C_{CB}, and the response to changes in coronary artery resistance (R_{COR}).

The system was again verified against the analytical model. The mean aortic pressure was found to have no significant difference ($p=0.16$) at 95% confidence and the waveform was well matched ($R^2=0.94$, $\sigma=10.2\%$). Q_{CV} was measured between the R_{CB} and the atrium tank (Figure 2.9) using a 30 mm circumference flow probe, which resulted in larger uncertainty than Q_{COR}, which used the 15 mm circumference flow probe. Overall, the results (Table 3.2) reveal acceptable agreement.

Table 3.2 Mean results for coronary system verification study. MCS values = mean ± uncertainty

Flow [Lpm]	**Analytical**	**MCS**
Cardiac Output (Q_{AO})	1.82	1.81 ± 0.01
Upper Body (Q_{UB})	0.37	0.37 ± 0.01
Lower Body (Q_{LB})	0.40	0.40 ± 0.01
Pulmonary (Q_{mBTS})	0.98	0.98 ± 0.01
Coronary Arterial (Q_{COR})	0.056	0.057 ± 0.002
Coronary Venous (Q_{CV})	0.056	0.056 ± 0.005
Pressure [mm Hg]	**Analytical**	**MCS**
Ascending Aorta (P_{AO})	60.11	60.65 ± 0.43
Coronary CA1 (P_{CA1})	53.63	54.15 ± 0.79
Coronary CA2 (P_{CA2})	43.72	43.94 ± 0.39
Coronary CB (P_{CB})	33.82	33.53 ± 0.55

The test section used in the MCS only requires an arterial CBF boundary condition. However, it is important to check that the coronary model can produce a venous CBF because the coronary LPN (Figure 2.9) was taken from the *in silico* Norwood model initially created by Lagana et al. [11]. Lagana et al. described creating the coronary LPN based on an adult mathematical model by Mantero et al. [13], who used the IMP methodology of Spaan et al. Thus, the *in vitro* coronary model was derived from the methodology of the IMP model proposed by Spaan et al. [31], whose main purpose was to accurately portray arterial and venous CBF. Testing reveals (Figure 3.7) that both arterial and venous CBF can be measured in the *in vitro* model.

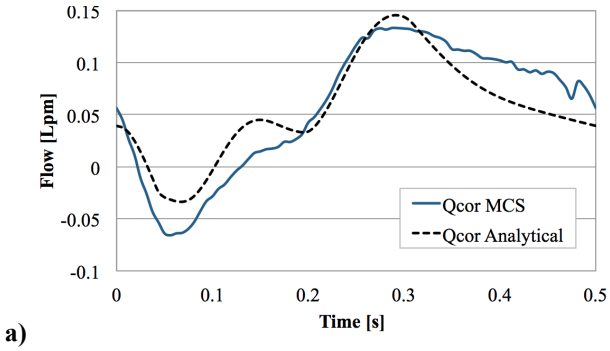

a)

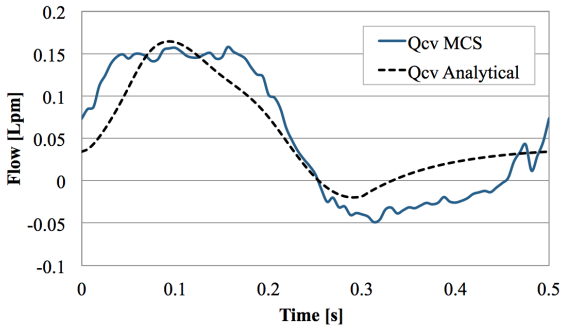

b)

Figure 3.7 Analytical and MCS (a) arterial Q_{COR} (R^2=0.86, σ=12.6%) and (b) venous Q_{CV} (R^2=0.85, σ=15.8%).

The waveforms for arterial Q_{COR} (R^2=0.86, σ=12.6%) and venous Q_{CV} (R^2=0.85, σ=15.8%) are in agreement with the analytical model. Furthermore, Spaan et al. described venous CBF mainly occurring in systole and minimally in diastole [31]. They explain that the coronary vessel's compliance attributes to a blood volume displacement: a diastolic filling of arterial CBF into the coronary bed, and a systolic emptying of that blood through the venous vessels [31]. This agrees with the analytical and MCS waveforms seen in Figure 3.7b: Q_{COR} and Q_{CV} are at their maximums in diastole and systole, respectively. Thus, the *in vitro* model is able to produce physiological venous and arterial CBF.

Once it was established that both arterial and venous CBF could be measured *in vitro*, the versatility of the CC was assessed. This was accomplished by changing the compliance (C_{CB}) of the CC by using different diaphragm materials. The diaphragm material's compliance (C_{CB}) cannot be directly measured, unlike air chambers whose air volume corresponds to a specific compliance. However, physical interaction with the material can reveal whether or not it is more or less flexible, which would mean more or less compliance. Thus, the material is iteratively chosen to achieve the desired analytical CBF waveform, which then correlates to an appropriately matched C_{CB}.

For testing, three diaphragm materials were used: a 0.003-inch thick latex, a 0.040-inch thick latex, and a 0.250-inch thick vulcanized silicone rubber. The flow measured using the 0.040-inch latex material from the verification study is labeled as Q_{COR} and Q_{CV} and corresponds to the C_{CB} value of 7.8E-3 mL/mmHg (Table 2.2). The more compliant and thinner 0.0025-inch latex CBF is labeled as Q_{COR+C} and Q_{CV+C}, and the less compliant 0.25-inch silicone rubber CBF is labeled as Q_{COR-C} and Q_{CV-C}. For comparison to the analytical model, a C_{CB} value of 7.8E-2 mL/mmHg and a C_{CB} value of 7.8E-4 mL/mmHg were shown to display the CBF waveform's response for more or less compliance, respectively. The MCS results for more and less compliance are not being directly compared to the analytical here. Instead, the comparison is the trend in which the flow waveforms respond to the changes in compliance C_{CB}. Through all testing, aortic pressure and SVP were held constant. The results for arterial CBF are seen in Figure 3.8.

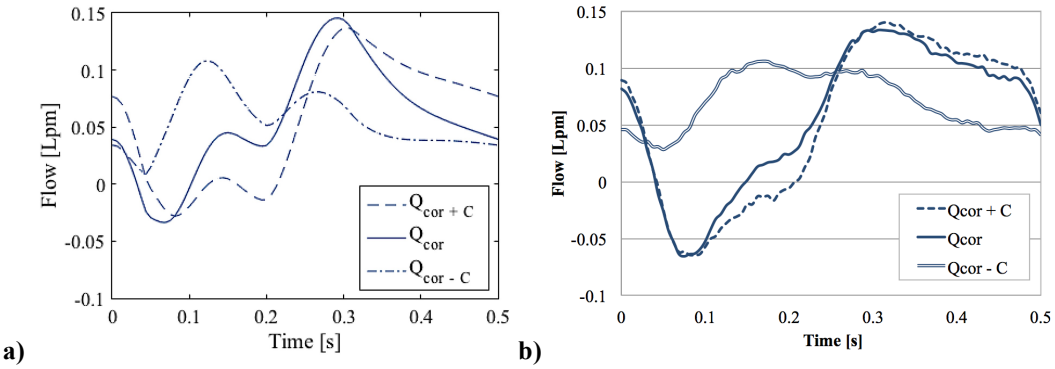

Figure 3.8 Results of varying C_{CB} for the (a) analytical and (b) *in vitro* arterial CBF (Q_{cor}).

Both the analytical and MCS results (Figure 3.8a and 3.8b) display the same response to changes in C_{CB}. Increasing the compliance (from $Q_{COR\ -\ C}$ up to $Q_{COR\ +\ C}$) results in decreased systolic flow and increased diastolic flow. Physiologically speaking, if the coronary vessels are more compliant (less stiff), then the intramyocardial pressure (or SVP) would more easily compress the vessels, obstructing the flow during systole. However, this more compliant vessel is then able to fill more during diastole. This is seen with Q_{COR+C}, which shows the most systolic retrograde flow and highest diastolic flow. Then when compliance is decreased, as in with Q_{COR-C}, there is less disrupted flow. For a less compliant myocardium, the SVP would have less effect on the flow since the rigid coronary vessels would not be as easily deformed under the intramyocardial pressure.

For venous CBF, Figure 3.9 shows that more flow occurs in systole for a more compliant coronary system (Q_{CV+C}). This agrees with results shown in Figure 3.8 where the most compliant CBF had the greatest diastolic flow. Hence, as Spaan et al. explained, more venous CBF is ejected from the coronary bed in systole when diastolic arterial CBF

is increased [31]. Additionally, the less compliant $Q_{CV\text{-}C}$ interacts similarly to $Q_{COR\text{-}C}$ where SVP appears to have minimal effect.

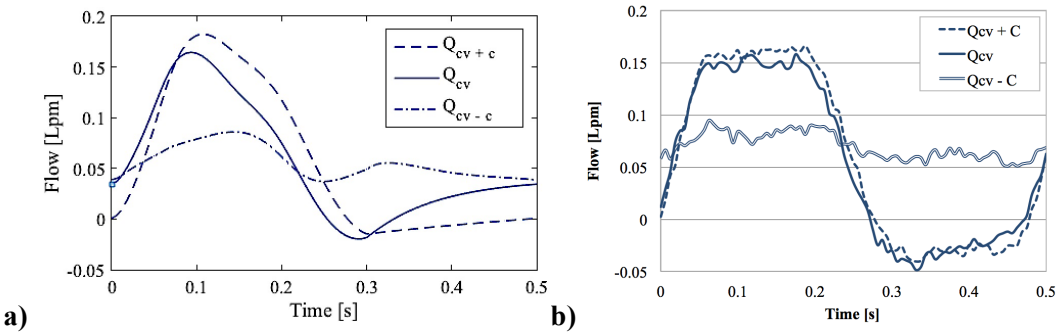

Figure 3.9 Results of varying C_{CB} for the (a) analytical and (b) *in vitro* venous CBF (Q_{cv}).

Next, the effect of resistance on the coronary circulation was evaluated. A flow resistor (pinch-needle valve) was placed between the test section's coronary artery and the CA1 impedance. This coronary artery resistance (R_{COR}) was increased from the reference setup while maintaining aortic pressure and SVP. The experimental and analytical results of resistance and flow are shown in Table 3.3. The flows from the reference setup are Q_{COR} and Q_{CV}, while $Q_{COR+Rcor}$ and $Q_{COR++Rcor}$ indicate increased resistance. Coronary artery resistance was calculated using Equation 3.7.

$$R_{COR} = (P_{AO} - P_{CA1})/Q_{COR} \tag{3.7}$$

Table 3.3 Resistance and flow for the MCS and analytical models (Results = mean ± uncertainty)

	Analytical R_{COR} [WU]	**MCS R_{COR} [WU]**	**Analytical Flow [Lpm]**	**MCS Flow [Lpm]**
Q_{COR}	117	112 ± 2	0.056	0.057 ± 0.002
$Q_{COR + Rcor}$	232	232 ± 2	0.050	0.049 ± 0.002
$Q_{COR ++ Rcor}$	691	691 ± 5	0.036	0.035 ± 0.002

The results of Table 3.3 had no statistical difference in their values ($p>0.05$). This is shown further in Figure 3.10 where the analytical and *in vitro* waveforms were highly correlated: Q_{COR+R} (R^2=0.87, σ=14.7%), Q_{CV+R} (R^2=0.87, σ=18.3%), Q_{COR++R} (R^2=0.89, σ=12.1%), and Q_{CV++R} (R^2=0.90, σ=14.1%). This indicates that the *in vitro* model has an accurate response to changes in coronary artery resistance using the flow resistor, whereas the resistance could have also been implemented by changing the structure of the test section's coronary artery.

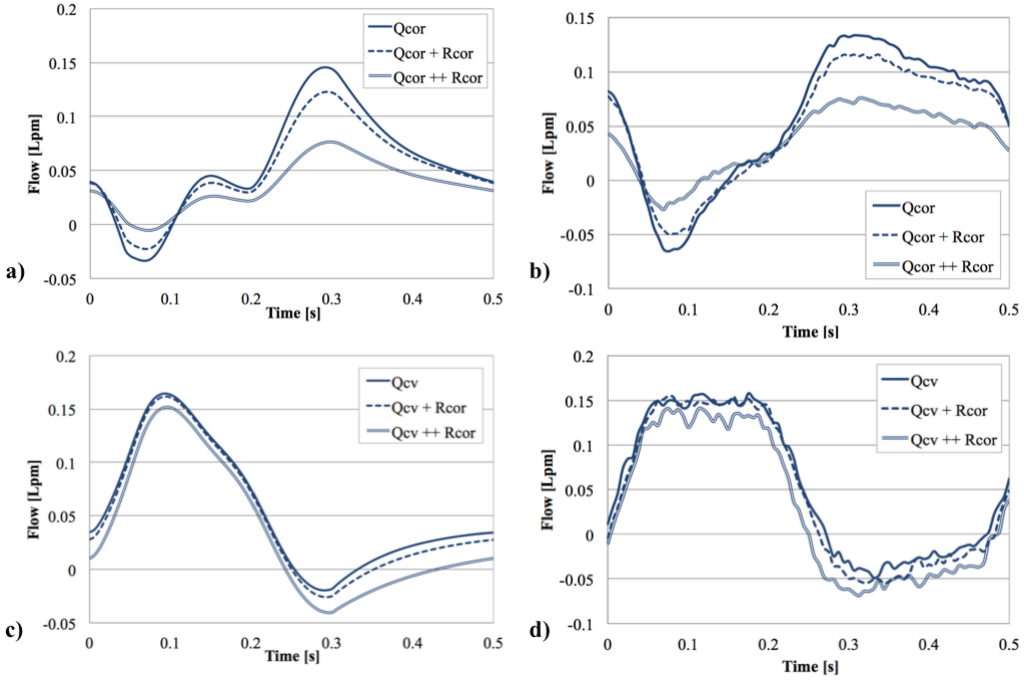

Figure 3.10 Arterial CBF for increasing R_{COR} for the (a) analytical and (b) *in vitro* models. Venous CBF for increasing R_{COR} for the (c) analytical and (d) *in vitro* models.

For arterial flow (Figures 3.10a-b), increased resistance decreased the systolic retrograde flow and decreased the total diastolic flow. For venous flow (Figures 3.10c-d), the increased resistance had a subtle effect of decreasing the total flow throughout the cardiac cycle. The overall effect was that total CBF decreased with increased R_{COR}, as

shown by Table 3.3. This is to be expected as the act of increasing R_{COR} has been used to model the effects of coronary artery stenosis. Mantero et al. modeled this in their study where increased R_{COR} resulted in increased systolic and decreased diastolic arterial CBF, with a total decreased CBF [13] (Figure 3.11).

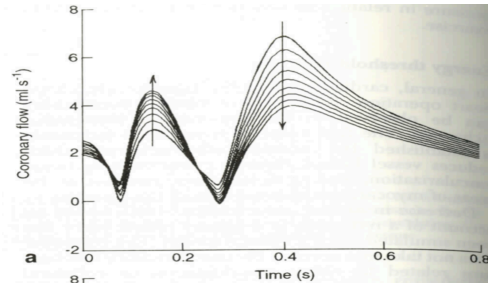

Figure 3.11 Coronary artery flow with increased resistance indicated by the arrows [13]

The results from Figures 3.10 and 3.11 indicate the importance of coronary stenosis and its effect on total CBF. For the present study, an addition of coronary stenosis (increased R_{COR}), or impeding the coronary artery in any way, would result in highly negative effects on the total CBF and thus myocardial oxygenation. This highlights the sensitivity of the coronary circulation to any change in the local resistance of the aortic arch and the importance of including it in the Norwood *in vitro* model.

Discussion

The verification study has shown that the *in vitro* MCS accurately reproduces the results predicted by the analytical model when tuned to similar conditions. Specifically, the *in vitro* coronary circulation produces physiological results for varying ranges of R_{COR} and changes in $C_{CB,}$ indicating the versatility of the SVP-C_{CB} coupling chamber.

Once it was established that the MCS was a capable model, it was then necessary to validate the model. A patient-specific study was used for this purpose.

CHAPTER FOUR

VALIDATION OF THE *IN VITRO* MODEL

The System Setup

In order to validate the MCS, it must be able to reproduce clinical data pertaining to a patient-specific setup (a LPN tuned to patient-specific impedance with an appropriate input aortic pressure waveform). This patient-specific study is necessary to ensure the MCS models physiological hemodynamics from which clinical implications can be obtained. And so, data from a HLHS patient (MUSC2) who received a 3.5mm diameter mBTS in the Norwood surgery was used for validation. A test section (Figure 4.1) was made based on medical imaging data of the blood volumes to incorporate the patient-specific structural characteristics of the reconstructed aortic arch.

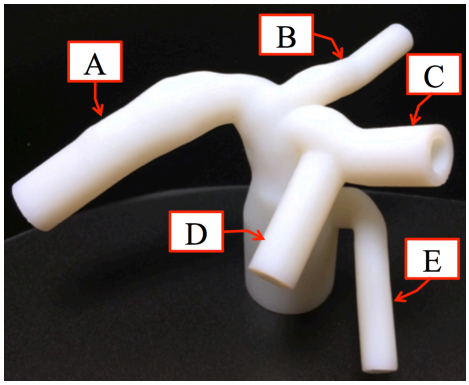

Figure 4.1 The MUSC2 3-D printed test section: (A) Descending Aorta, (B) LCA, (C) Innominate artery, (D) mBTS, (E) Coronary artery

Figure 4.1 shows the 3-D printed MUSC2 test section of the reconstructed aortic arch. Similar to the model used in the verification study, a representative coronary artery (2 mm inner diameter) was placed at the site of the DKS anastomosis (Figure 4.1 E). Any

flow towards the DKS was assumed to go to the coronary circulation, similar to the assumption by Corsini et al. [43]. Additionally, the MUSC2 model does not have an LSA, which was disconnected during Stage 1 surgery. However, it is common for the body to adjust for this change by creating connections at more distal points within the vasculature [22]. And so, the resistance and compliance of the LSA was incorporated into the LCA, resulting in the LPN of the MCS seen in Figure 4.2.

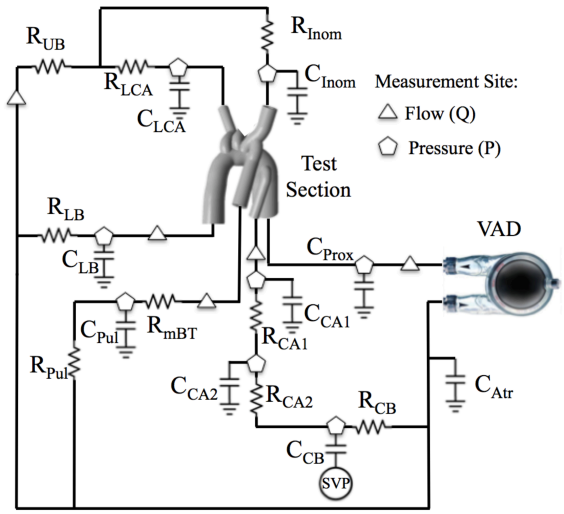

Figure 4.2 Schematic of the MCS used for the MUSC2 validation study.

The clinical data provides flow estimates for the cardiac output, upper body, lower body, and mBTS/pulmonary. However, because coronary flow is not typically measured *in vivo* during Stage 1 surgery, the flow had to be estimated. It was previously stated that coronary flow is approximately 4% of the cardiac output [15]. This would result in 0.0504 Lpm for the MUSC2 Q_{COR}. Additionally, Duncker et al. showed that Q_{COR} per gram of myocardium [mL/min-g] could be related to heart rate (HR) [bpm] using Equation 4.1 [16].

$$\frac{Q_{COR}}{Myocardium\ Weight} = 0.016 * HR - 0.30 \quad (4.1)$$

Rastin et al. also proposed that myocardium weight could be estimated based on patient weight [44]. The MUSC2 patient had a weight of 5.4 Kg and so the estimated myocardium weight was 30 g. Together with the heart rate of 120 bpm, the CBF was calculated using Eq. 4.1 to be 0.486 Lpm. This value was approximately 3.9% of the cardiac output for MUSC2. Based on the two methods of estimating CBF, an average of the two results was taken, resulting in target Q_{COR} of 0.050 Lpm for MUSC2. To account for this flow in the cardiac output and satisfy continuity, the estimated Q_{COR} was subtracted from Q_{UB} and Q_{LB} equally. This was done because clinical data of cardiac output and mBTS flow waveforms were to be matched in the validation study, whereas upper and lower body flows were not. Adding or subtracting Q_{COR} from the mean Q_{AO} and Q_{mBTS} would have tainted the validation efforts, as well as change the target clinical Q_P/Q_S.

The MUSC2 model has a BSA of 0.30 m^2. The LPN values for the coronary circulation (Appendix B) were scaled according to the methods proposed by Pennati and Fumero [40]. The coronary resistance values and the estimated Q_{COR} were then used to estimate the mean pressures P_{CA1}, P_{CA2}, and P_{CB}. The SVP minimum and maximum pressures were adjusted based on the clinical mean atrium pressure and maximum clinical systolic aortic pressure. Systolic time for the SVP was based on the notion that ventricular pressure rises slightly before aortic pressure during isovolumetric contraction. Additionally, the descent of the SVP was adjusted to cross the dichrotic notch of the

clinical $P_{AO.}$ This completed the parameters necessary for setting up the MUSC2 coronary circulation.

To account for the viscous effects of blood in the test section, a glycerin solution (58% water and 42% glycerin) was used as a blood analog. This mixture resulted in a density of 1096 kg/m^3, a kinematic viscosity of 3.85 cS, and a dynamic viscosity of 4.21 cP. These values fell within clinical ranges for blood and those used by the *in silico* Norwood studies [9, 10]. Additionally, the heart rate was 120 bpm, resulting in a 0.50 second cardiac cycle. All flow and pressure measurements were measured using the same equipment and methods from the verification study (see Appendix A). The MUSC2 pre-Glenn catheterization and echo data were used to match aortic pressure, cardiac output, and mBTS flow waveforms. Results were analyzed using the same methods proposed in the verification study (See Appendix C for details).

Validation Results

The results of the MUSC2 validation study can be seen in Tables 4.1 and 4.2. Statistically significant differences ($p<0.05$) are considered clinically insignificant if they met the following criteria: mean pressure was within 1 mmHg of *in vivo* measurement or if the mean flow's uncertainty encompassed the clinical value. This was assumed because *in vivo* flow uncertainty is unknown but usually taken to be within 10%, and pressure measurement resolution is 1 mmHg.

Table 4.1 Mean results of the MCS validation test compared against mean clinical values. and the estimated mean coronary values. MCS values = mean ± uncertainty

Flow [Lpm]	**Clinical**	**MCS**	**Resistance [WU]**	**Clinical**	**MCS**
Cardiac Output (Q_{AO})	1.26	1.25 ± 0.01	Upper Body (UBSVR)	170	175 ± 6
Upper Body (Q_{UB})	0.31	0.30 ± 0.01	Lower Body (LBSVR)	166	169 ± 6
Lower Body (Q_{LB})	0.32	0.31 ± 0.01	mBTS (R_{mBTS})	80	79 ± 1
Pulmonary (Q_{mBTS})	0.58	0.58 ± 0.01	Pulmonary (R_{pul})	10	11 ± 0.2
Pressure [mm Hg]	**Clinical**	**MCS**	**Pressure [mm Hg]**	**Clinical**	**MCS**
Ascending Aorta (P_{AO})	58.76	58.99 ± 0.30	Pulmonary (P_{pul})	12.00	12.61 ± 0.06

Table 4.2 Mean results of the MCS validation test compared against the estimated mean coronary values. MCS values = mean ± uncertainty

Flow [Lpm]	**Estimated**	**MCS**
Coronary (Q_{COR})	0.050	0.049 ± 0.002
Pressure [mm Hg]	**Estimated**	**MCS**
Coronary CA1 (P_{CA1})	52.33	51.86 ± 0.26
Coronary CA2 (P_{CA2})	42.55	41.86 ± 0.21
Coronary CB (P_{CB})	32.77	30.39 ± 0.15
Resistance [WU]	**Estimated**	**MCS**
Coronary Artery (R_{COR})	129	144 ± 6
Coronary CA1 (R_{CA1})	196	203 ± 8
Coronary CA2 (R_{CA2})	196	232 ± 10
Coronary CB (R_{CB})	535	494 ± 20
Total Coronary (R_{TC})	1055	1073 ± 44

From Tables 4.1 and 4.2, the mean results are in good agreement and differences considered insignificant based on the stated criteria. For instance, the cardiac output (Q_{AO}) was found to have statistical difference in means ($p<0.05$), however the uncertainty of the MCS value included the clinical reference value. Additionally, the Q_{AO} clinical and MCS waveforms were reasonably correlated ($R^2=0.91$, $\sigma=9.9\%$). The Q_{mBTS} waveforms were also highly correlated ($R^2=0.96$, $\sigma=13.5\%$) and found to have no statistical difference in means ($p=0.15$). These flow waveforms are seen in Figure 4.3.

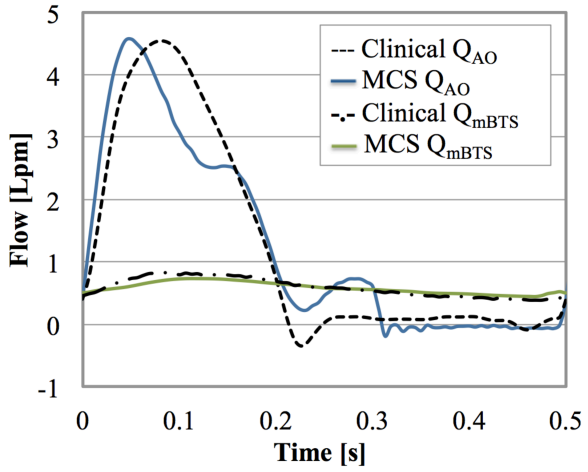

Figure 4.3 Clinical and MCS aortic flow (R^2=0.91, σ=9.9%) and mBTS flow (R^2=0.96, σ=13.5%)

The MCS and clinical aortic pressure waveforms (Figure 4.4) also reveal high correlation (R^2=0.97, σ=6.0%). Mean P_{AO} results did reveal statistical differences ($p<0.05$), however the MCS value was within 1 mmHg of the clinical. Additionally, the clinical and MCS aortic pulse pressures are 64.8 mmHg and 66.5 mmHg, respectively. For the systolic portion of $P_{AO,}$ the clinical dP/dt is 838 mmHg/s and the MCS dP/dt is 824 mmHg/s.

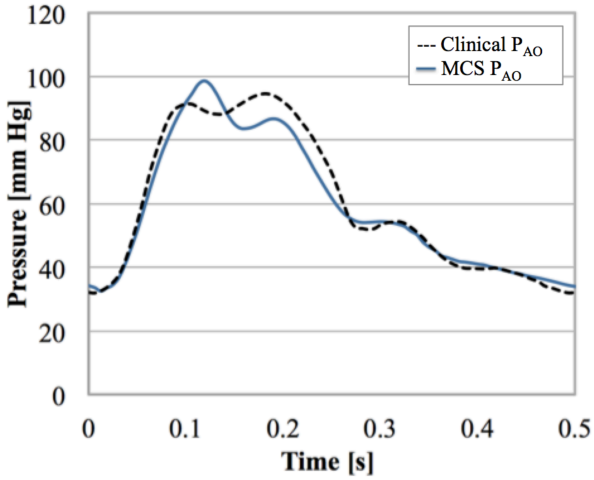

Figure 4.4 Clinical and MCS aortic pressure waveforms (R^2=0.97, σ=6.0%)

The proximal compliance (C_{Prox}) is used to provide compliance to the rigid test section, and thus shape the aortic pressure waveform. The MSC C_{Prox} was measured to be 0.082 mL/mmHg. While there are no clinical compliance values available, scaling C_{Prox} from the verification model would result in a value of 0.084 mL/mmHg. The similarity of these values is noteworthy considering that the verification test section was derived from the MUSC2 patient [10]. The additional MCS compliance values are seen in Table 4.3 where they are compared to the scaled compliance values of the verification LPN. C_{CB} scaled to a value of 0.0068 mL/mmHg, compared to the verification model's C_{CB} of 0.0078 mL/mmHg. The difference in values was determined to be indistinguishable between different C_{CB} materials and so the same 0.040-inch thick latex rubber was used for C_{CB}.

Table 4.3 Experimental compliance values of the validation study relative to scaled values from the verification model. Compliance (C) [mL/mmHg]

	C_{Prox}	C_{Pul}	C_{LB}	C_{Inom}
MCS	0.082 ± .006	0.29 ± .08	0.081± .009	0.117± .011
BSA Scaled	0.084	0.34	0.069	0.078
	C_{LCA}	C_{CA1}	C_{CA2}	
MCS	0.115 ± .008	0.00025 ± 0.00012	0.00050 ± 0.00013	
BSA Scaled	0.078	0.00017	0.00046	

As shown in Table 4.3, there are notable similarities in the validation MCS's compliance values and those estimated by the analytical model from the verification study. This, along with the Table 4.1 results and the highly correlated waveforms, supports the notion that the MCS is validated against clinical data. Additionally, the MCS Q_{COR} (Table 4.2) was found to have no statistical difference (p=0.51) from the estimated Q_{COR}. The resistances (Table 4.2) through the coronary circulation were well matched,

resulting in coronary pressures consistent with the predicted values. Lastly, the Q_{COR} waveform displayed the same coronary flow characteristics that were expected. These are seen in Figure 4.5 with respect to the aortic pressure and the arterial coronary pressure, P_{CA1}.

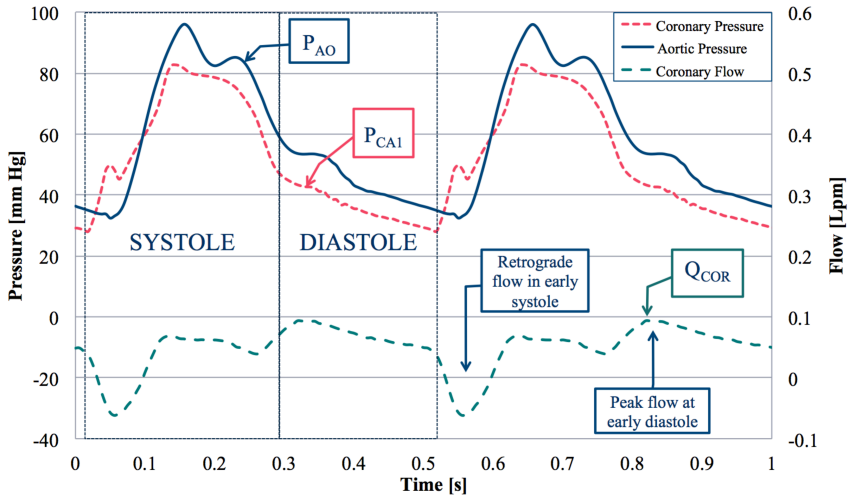

Figure 4.5 The Q_{COR} waveform (Right axis) in relation to P_{AO} and P_{CA1} waveforms (Left axis).

In Figure 4.5, Q_{COR} during early systole displays a slight retrograde flow. As shown by P_{CA1}, this is caused by the increase in intramyocardial pressure during the isovolumetric contraction of the cardiac cycle. In the isovolumetric time period there is no cardiac output and the aortic pressure is low. Once the aortic flow starts, the aortic pressure rises and offsets the coronary perfusion pressure to allow for an increase in Q_{COR}. However, it isn't until diastole that the intramyocardial pressure drops and P_{CA1} falls substantially. This difference in P_{CA1} and P_{AO} allows for the sharp increase in Q_{COR}. Consequently, the Q_{COR} waveform for the validation case is physiologically accurate.

Discussion

The clinical reference data was recapitulated by the *in vitro* MCS, all while incorporating an *in vitro* coronary system that produced physiological results. It can therefore be concluded that the MCS is a validated system. However, with regards to how the coronary system is performing, a single validation case cannot define clinical implications. The CBF was purely estimated and can only be used as a reference point. To obtain meaningful relationships between the coronary flow and the rest of the MCS, a parametric study must be performed.

CHAPTER FIVE

MBTS PARAMETRIC STUDY

Purpose

The Norwood procedure using the mBTS is notorious for its negative effects on coronary perfusion. *In silico* studies [8–11] have explicitly related mBTS size to coronary perfusion pressure, flow, and the overall balance of pulmonary and systemic flow (Q_P/Q_S), factors crucial to a Norwood patient's survival. As previously mentioned, no *in vitro* model has studied this relationship, which brings about the purpose of this parametric study. By obtaining *in vitro* results for the effects of changing mBTS size on coronary hemodynamics, the results can confirm or negate those presented by the *in silico* models. These results, regardless of the agreement, can then be used for clinical implications.

Testing Methods

The inner diameter of the mBTS was used as the varying parameter in this study. The MUSC2 patient-specific test section and setup from the validation study (Figure 4.2) was used as the reference case from which mBTS changes were made. As the reference MUSC2 test section had a 3.5mm mBTS, two other models were created with a 3mm mBTS and 4mm mBTS. These values are the typical sizes used in studies evaluating mBTS size effects, and so they were used here for comparison to such studies [8–11]. It is also important to note that because the validated MCS of a 3.5 mm mBTS patient used

estimated coronary hemodynamics, the parametric study's coronary results should only be viewed relative to the 3.5 mm mBTS results.

The initial test was using the 3.5mm mBTS, and was essentially another validation case. Then the test section would be interchanged with another of a different mBTS size. The resistance, compliance, and atrium pressure of the 3.5mm test setup were held constant throughout all test section changes. For the 3mm and 4mm mBTS models, the first two cases studied were maintaining the mean aortic pressure and maintaining the cardiac output of the 3.5mm mBTS case. By maintaining the aortic pressure and thus upper body flow, this simulated the idea of constant cerebral perfusion (maintaining the original blood flow to the brain). Any changes in aortic pressure were also adjusted-for in the SVP: if peak systolic P_{AO} increased/decreased, then SVP would increase/decrease accordingly.

Under the same testing conditions, an additional study looked at maintaining the ratio VP/CBF for all shunt sizes. This ratio (Equation 5.1) relates the ventricle power output (VP) to the supply of coronary blood (CBF).

$$VP/CBF = \left(\frac{1}{t_c} \int_0^{t_c} \overline{P_{AO} Q_{AO}}(t) dt \right) / Q_{COR} \tag{5.1}$$

where t_c is the time for one cardiac cycle, $\overline{P_{AO} Q_{AO}}(t)$ is the ensembled product of P_{AO} and Q_{AO} at each point in the cardiac cycle, and Q_{COR} is the mean CBF.

The Norwood heart has limited myocardial oxygen reserve [12], meaning that there isn't much ability for the myocardium to extract more oxygen for the same amount of

coronary blood provided. CBF provides the oxygen to the heart so that it can contract and produce work. By maintaining the ratio of power output for a given amount of CBF, this simulates the heart not working more or less for the amount of "energy" provided.

All testing for each shunt model was performed during the same testing session to ensure consistency between the tuned system parameters and VAD. The same system tuning and data recording methods as the verification and validation studies were used in the parametric study (Appendix A). Results were analyzed using the previously stated methods for the verification and validation studies (Appendix C).

Results for Constant Cardiac Output

Table 5.1 presents the results from the 3.5 mm mBTS setup. It was important to obtain clinical validation of the MCS results before comparing to the 3 mm and 4 mm mBTS results. In doing so, changes using the different sized shunts would be relative to clinical values.

Table 5.1 Results for the 3.5mm mBTS system setup. MCS = Mean ± Uncertainty

Flow [Lpm]	**Clinical**	**MCS**	**Flow [Lpm]**	**Estimated**	**MCS**
Cardiac Output (Q_{AO})	1.26	1.27 ± 0.01	Coronary (Q_{COR})	0.050	0.051 ± 0.002
Upper Body (Q_{UB})	0.31	0.31 ± 0.01	**Pressure [mmHg]**	**Estimated**	**MCS**
Lower Body (Q_{LB})	0.32	0.32 ± 0.01	Coronary CA1 (P_{CA1})	52.33	52.83 ± 0.26
Pulmonary (Q_{mBTS})	0.58	0.58 ± 0.01	Coronary CA2 (P_{CA2})	42.55	43.04 ± 0.21
Pressure [mm Hg]	**Clinical**	**MCS**	Coronary CB (P_{CB})	32.77	32.28 ± 0.15
Ascending Aorta (P_{AO})	58.76	58.63 ± 0.30	**Resistance [WU]**	**Estimated**	**MCS**
Pulmonary (P_{pul})	12	11.96 ± 0.06	Coronary Artery (R_{COR})	129	114 ± 4
Atrium (P_{Atr})	6	6.02 ± 0.06	Coronary CA1 (R_{CA1})	196	193 ± 8
Resistance [WU]	**Clinical**	**MCS**	Coronary CA2 (R_{CA2})	196	212 ± 8
Upper Body (UBSVR)	170.2	169 ± 5	Coronary CB (R_{CB})	535	517 ± 20
Lower Body (LBSVR)	165.9	164 ± 5	Total Coronary (R_{TC})	1055	1055 ± 41
mBTS (R_{mBTS})	80.1	80 ± 1			
Pulmonary (R_{pul})	10	10 ± 0.2			

The mean results of Table 5.1 are in good agreement with the clinical and estimated values, illustrating the MCS's repeatability. No clinical significance in data was detected. The P_{AO} clinical and MCS waveforms were reasonably fitted (R^2=0.90, σ=11.7%). The Q_{AO} waveforms were well matched (R^2=0.97, σ=7.3%), as were the Q_{mBTS} waveforms (R^2=0.95, σ=9.7%). These are seen in Figure 5.1.

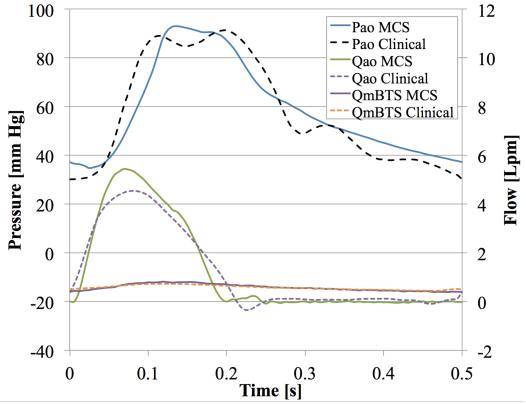

Figure 5.1 Parametric study validation waveforms of Q_{AO}, Q_{mBTS}, and P_{AO}.

Once it was established that the MCS was working under the correct clinical conditions, the test sections were interchanged. Cardiac output was maintained by adjusting the aortic pressure using the VAD and the resulting hemodynamics were recorded (Table 5.2).

Table 5.2 Parametric study results for constant cardiac output. Mean results for flow [Lpm] and pressure [mmHg]. (Bottom three rows) Percent change relative to the 3.5mm values.

mBTS	Q_{COR}	Q_{mBTS}	Q_{UB}	Q_{LB}	Q_P / Q_S	P_{AO}
3 mm	0.053 ± 0.002	0.56 ± 0.01	0.33 ± 0.01	0.33 ± 0.01	0.79	61.8 ± 0.3
3.5 mm	0.051 ± 0.002	0.58 ± 0.01	0.31 ± 0.01	0.32 ± 0.01	0.85	58.6 ± 0.3
4 mm	0.048 ± 0.002	0.61 ± 0.01	0.30 ± 0.01	0.31 ± 0.01	0.92	55.2 ± 0.3
mBTS	**Q_{COR}**	**Q_{mBTS}**	**Q_{UB}**	**Q_{LB}**	**Q_P / Q_S**	**P_{AO}**
3 mm	5%	-4%	3%	3%	-7%	5%
3.5 mm	-	-	-	-	-	-
4 mm	-6%	4%	-3%	-3%	8%	-6%

From Table 5.2, increasing the mBTS from a 3mm to a 4mm size and maintaining the cardiac output required a large decrease in the mean P_{AO} to account for the decreased total MCS resistance. Further, as shunt size increased, the Q_{mBTS} also increased while the systemic circulation suffered. This is shown individually through the decreased Q_{UB}, Q_{LB}, and Q_{COR}, with the total effect shown by the large increase in Q_P/Q_S.

Additionally, all mean values of Table 5.2 were found to have significant difference ($p<0.05$) between the different mBTS sizes. The most notable difference is seen in the percent change of coronary flow. The variation in mBTS caused a span of 11% change (from 3mm to 4mm) in Q_{COR}. This disparity can better be seen in Figure 5.2 of the aortic pressure, coronary flow, and mBTS flow waveforms.

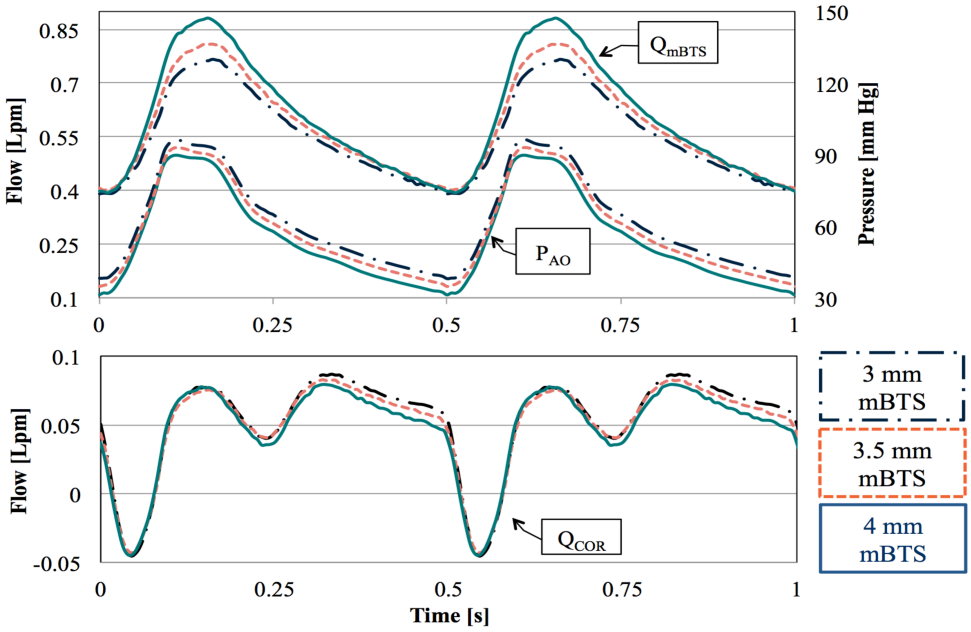

Figure 5.2 Waveforms for P_{AO}, Q_{mBTS}, and Q_{COR} for the varying shunt sizes while held at constant cardiac output.

Figure 5.2 shows that as the mBTS size increased, the systolic and diastolic Q_{mBTS} increased. To maintain the cardiac output, the peak systolic P_{AO} decreased while also

decreasing the diastolic aortic pressure. Because the systolic P_{AO} decreased, the SVP also decreased its peak systolic pressure. Therefore, the difference in Q_{COR} is not as evident during systole. However, in diastole, because the diastolic aortic pressure decreased with increased mBTS size, the diastolic Q_{COR} also decreased due to the reduced perfusion pressure, CPP. Seeing as Q_{mBTS} increased in the diastolic time period while Q_{COR} decreased, this indicates the "shunt stealing" [9] phenomenon.

Results for Constant Aortic Pressure

In a similar manner to the constant cardiac output study, results were obtained for the different mBTS sizes while maintaining the mean aortic pressure. These results can be seen in Table 5.3.

Table 5.3 Parametric study results for constant aortic pressure. Mean results for flow [Lpm] and pressure [mmHg]. (Bottom three rows) Percent change relative to the 3.5mm values.

mBTS	Q_{COR}	Q_{mBTS}	Q_{UB}	Q_{LB}	Q_{AO}	Q_P / Q_S
3 mm	0.051 ± 0.002	0.54 ± 0.01	0.31 ± 0.01	0.32 ± 0.01	1.22 ± 0.01	0.79
3.5 mm	0.051 ± 0.002	0.58 ± 0.01	0.31 ± 0.01	0.32 ± 0.01	1.27 ± 0.01	0.85
4 mm	0.050 ± 0.002	0.63 ± 0.01	0.32 ± 0.01	0.32 ± 0.01	1.32 ± 0.01	0.91
mBTS	Q_{COR}	Q_{mBTS}	Q_{UB}	Q_{LB}	Q_{AO}	Q_P / Q_S
3 mm	0%	-7%	0%	0%	-4%	-7%
3.5 mm	-	-	-	-	-	-
4 mm	-1%	9%	1%	0%	4%	8%

The mean results of maintaining aortic pressure (Table 5.3) are not as dramatic as those of maintaining cardiac output (Table 5.2). As the MCS's resistance, except for the shunt, stayed the same with each varying mBTS test section, maintaining aortic pressure should result in no change in the mean flows to each region where resistance didn't change. Thus, the systemic flow results do not reveal any noteworthy differences. The

only notable changes are with Q_{AO}, Q_{mBTS}, and Q_P/Q_S. In fact, when maintaining aortic pressure, the relative change in Q_{mBTS} is much more noticeable. However, comparing the Q_P/Q_S of Table 5.2 and Table 5.3, the same relative changes were achieved. This reveals that regardless of whether the heart works to maintain cardiac output or aortic pressure, the Q_p/Q_S is highly sensitive to the mBTS size.

Results for Constant Ventricle Power per Coronary Flow

The results of maintaining the VP/CBF are seen in Table 5.4. The results of VP and VP/CBF are also shown for the other cases. Note that VP/CBF for the constant cardiac output case of the 3mm mBTS resulted in the same VP/CBF ratio as the 3.5mm mBTS.

Table 5.4 Parametric study results for constant SVP/CBF [J/L]. Mean flow (Q) [Lpm], Mean pressure (P) [mmHg], Ventricle Power (VP) [mW]. Test results from the constant Q_{AO} and mean P_{AO} cases are denoted by "CO" and "P", respectively. A * is used to denote constant VP/SVP (Bottom three rows) Percent change relative to the 3.5mm values.

mBTS	Q_{COR}	Q_{AO}	P_{AO}	Q_{mBTS}	Q_P/Q_S	VP	VP/CBF
3 mm P	0.051 ± 0.002	1.22 ± 0.01	58.8 ± 0.3	0.54 ± 0.01	0.79	187.1	220.2
3 mm CO *	0.053 ± 0.002	1.27 ± 0.01	61.8 ± 0.3	0.56 ± 0.01	0.79	205.3	231.3
3.5 mm	0.051 ± 0.002	1.27 ± 0.01	58.6 ± 0.3	0.58 ± 0.01	0.85	196.3	231.9
4 mm *	0.047 ± 0.002	1.25 ± 0.01	53.9 ± 0.3	0.60 ± 0.01	0.92	180.2	231.9
4 mm CO	0.048 ± 0.002	1.27 ± 0.01	55.2 ± 0.3	0.61 ± 0.01	0.92	187.7	236.7
4 mm P	0.050 ± 0.002	1.32 ± 0.01	58.8 ± 0.3	0.63 ± 0.01	0.91	208.7	250.3
mBTS	**Q_{COR}**	**Q_{AO}**	**P_{AO}**	**Q_{mBTS}**	**Q_P/Q_S**	**VP**	**VP/CBF**
3 mm P	0%	-4%	0%	-7%	-7%	-5%	-5%
3 mm CO *	5%	0%	5%	-4%	-7%	5%	0%
3.5 mm	-	-	-	-	-	-	-
4 mm *	-8%	-2%	-8%	3%	8%	-8%	0%
4 mm CO	-6%	0%	-6%	4%	8%	-4%	2%
4 mm P	-1%	4%	0%	9%	8%	6%	8%

From Table 5.4, when maintaining VP/CBF and decreasing the shunt size to 3mm, there is a 5% increase in CBF and ventricle power. However, there is a 7% decrease in

Q_P/Q_S, which would result in a less oxygen saturation rates for the CBF. The combination of decreased saturation rates and increased power are unfavorable for the single ventricle heart. Likewise, when the mBTS is increased to 4mm, there is an 8% loss of CBF with an 8% decrease in VP. This also results in a drop (2% decrease) in cardiac output. Lower Q_{AO} coupled with the increased (8%) Q_P/Q_S results in a drop in systemic blood flow, which may be problematic for cerebral perfusion.

Lastly, consider if the heart were to attempt to increase CBF to the initial 3.5mm case value, as in the "4 mm P" scenario. The heart would then have to increase VP by 6%, resulting in an increase of the ratio VP/CBF by 8%. As the myocardium has limited oxygen extraction reserve [12], it is likely unrealistic to consider this situation where the heart would work harder for the same amount of CBF provided.

Discussion and Clinical Implications

The results of this *in vitro* study reveal that as shunt size (the inner diameter of the mBTS) increases in a Norwood patient, the blood flow to the myocardium (CBF) decreases. Figure 5.2 shows that CBF and diastolic P_{AO} decrease with increasing mBTS size. CBF is dependent on the CPP, as well as the ventricular contraction's interaction with the coronary vasculature [18]. In this study, changes in the ventricular contraction are accounted for using the SVP-C_{CB} coupling chamber by adjusting the SVP. That is why Figure 5.2 did not reveal a substantial difference in CBF during systole; as systolic P_{AO} increased so did SVP. The real difference was in diastole where ventricular contraction (and so SVP) has its least restraining effect on CBF, and CPP is the main

dictator of how much Q_{COR} there is. Thus, because diastolic P_{AO} decreases with increasing mBTS size, CPP decreases and there is less Q_{COR}.

Table 5.4 shows that as mBTS size increases the ratio of pulmonary to systemic blood flow (Q_P/Q_S) also increases. While this may lead to a better balance of oxygenated and deoxygenated blood in the Norwood patient, the myocardium is still receiving less blood flow, particularly in the 4mm case of constant VP/CBF. The myocardium's oxygen extraction capabilities are limited [21]. So, in the condition that the heart would either maintain a certain amount of cardiac output or maintain the VP/CBF after Norwood palliation, a shunt too large in size would result in a relatively lower CBF.

In order to increase the CBF with the larger shunt, issues arise with the systolic P_{AO} and required ventricle power. This idea was shown through the constant aortic pressure tests where coronary blood flow was maintained for the various mBTS sizes. While mean P_{AO} is the same between all shunt sizes, the aortic pressure waveforms reveal that systolic pressure increases and diastolic pressure slightly decreases with increasing shunt size. This can be seen in Figure 5.3 of P_{AO} for various shunt sizes at a constant mean P_{AO}.

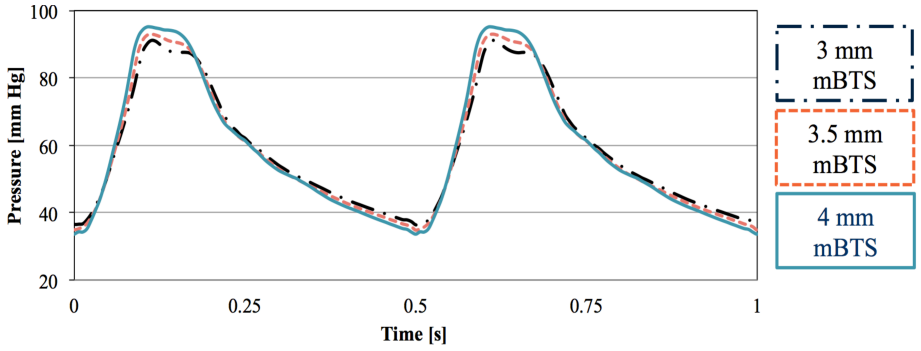

Figure 5.3 Waveforms for P_{AO} for the varying shunt sizes while maintaining the average P_{AO}.

In maintaining mean P_{AO} and CBF, Figure 5.3 reveals the change in shunt size, and thus impedance of the circulation, changes the form of P_{AO}. The systolic P_{AO} and SVP increase with the larger mBTS. The increased SVP increases myocardial work and oxygen demand [21]. This idea is also shown through the 6% increase in ventricle power and 8% in VP/CBF from Table 5.5. So in the case where the heart attempted to maintain a certain cardiac output there was less CBF. If the heart were to increase the CBF, then the results reveal that the systolic peak, cardiac output, and thus power output would have to increase. This idea is also illustrated with Figure 5.4.

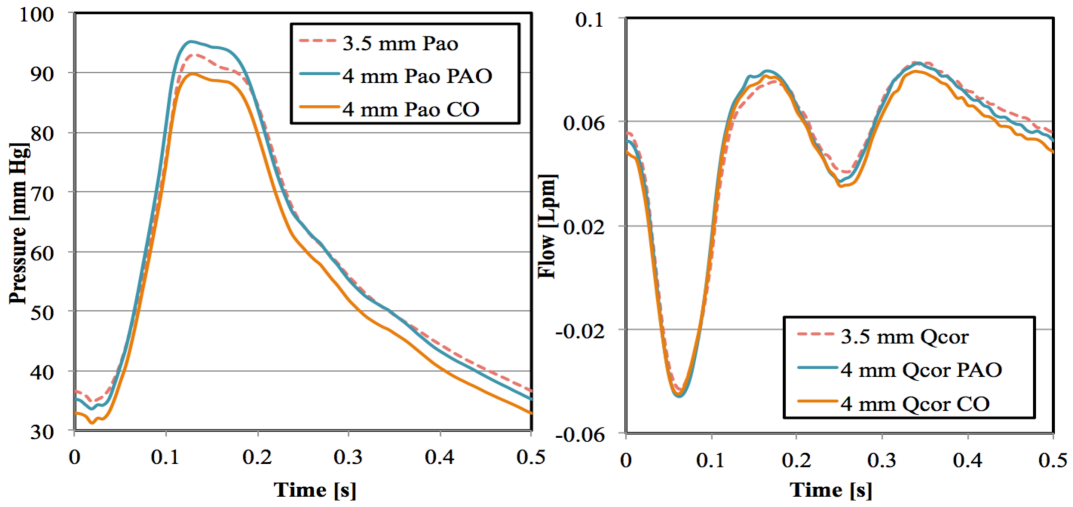

Figure 5.4 Waveforms for P_{AO} and Q_{COR} for the reference 3.5mm shunt size and the 4 mm shunt size. Labels with "PAO" are from the constant aortic pressure test and labels with "CO" are from the constant cardiac output test.

Figure 5.4 shows that when the mBTS size was increased, CBF and P_{AO} decreased for the constant cardiac output case. When P_{AO} was increased to achieve the same CBF as the 3.5 mm mBTS case, the systolic P_{AO} increased ("4 mm P_{AO} PAO" in Fig. 5.4). From Table 5.4, the 4mm mBTS with constant mean aortic pressure had a 6% increase in VP and 8% increase in VP/CBF. This means that the heart would be working harder and

demanding more oxygen for essentially the same amount of CBF as the 3.5 mm case. This could result in a devastating cyclic reaction where the heart continues to work harder to increase CBF but isn't able to supply enough oxygen to the myocardium for the amount of work performed. As the Norwood heart is already a single ventricle system having undergone highly invasive modifications, it is advised that caution is given to how mBTS size can affect CBF and ventricular function.

In silico studies [7–9, 11] have expressed the detrimental effects of the mBTS on Norwood hemodynamics, in particular to coronary perfusion. Specifically, Table 5.5 shows that as mBTS size increases, coronary blood flow decreases and Q_P/Q_S increases.

Table 5.5 *In silico* [7], [9], [11] **and *in vitro* MCS results of varying mBTS size. Top three rows: Flow (Q) [Lpm] and pressure (P) [mmHg]. Bottom three rows: Changes relative to the 3.5mm results.**

Bove et al. [7]					**Moghadam et al.** [9]				
mBTS	Q_{AO}	P_{AO}	Q_{COR}	Q_P/Q_S	**mBTS**	Q_{AO}	P_{AO}	Q_{COR}	Q_P/Q_S
3 mm	2.12		0.081	0.72	**3 mm**	2.09		0.0854	0.726
3.5 mm	2.28		0.076	1	**3.5 mm**	2.23		0.0796	1.004
4 mm	2.38		0.071	1.26	**4 mm**	2.35		0.0741	1.302
	Q_{AO}	P_{AO}	Q_{COR}	Q_P/Q_S		Q_{AO}	P_{AO}	Q_{COR}	Q_P/Q_S
3 mm	-7%		7%	-28%	**3 mm**	-6%		7%	-28%
3.5 mm	-	-	-	-	**3.5 mm**	-	-	-	-
4 mm	4%		-7%	26%	**4 mm**	5%		-7%	30%
Lagana et al. [11]					***in vitro* MCS**				
mBTS	Q_{AO}	P_{AO}	Q_{COR}	Q_P/Q_S	**mBTS**	Q_{AO}	P_{AO}	Q_{COR}	Q_P/Q_S
3 mm	2.123	84.56	0.082	0.72	**3 mm**	1.27	61.76	0.053	0.79
3.5 mm	2.275	79.83	0.076	1.003	**3.5 mm**	1.27	58.63	0.051	0.85
4 mm	2.387	75.67	0.071	1.254	**4 mm**	1.27	55.17	0.048	0.92
	Q_{AO}	P_{AO}	Q_{COR}	Q_P/Q_S		Q_{AO}	P_{AO}	Q_{COR}	Q_P/Q_S
3 mm	-7%	6%	8%	-28%	**3 mm**	0%	5%	5%	-7%
3.5 mm	-	-	-	-	**3.5 mm**	-	-	-	-
4 mm	5%	-5%	-7%	25%	**4 mm**	0%	-6%	-6%	8%

These *in silico* results of Table 5.5 are consistent with the *in vitro* findings in the present study, which reveals two important conclusions. The first is that since the *in silico* results agree with the *in vitro* results, the *in silico* results are verified and can be used for clinical implications. The second is that both results reveal the negative effects of increasing mBTS size, which could lead to the demise of the Norwood heart.

CHAPTER SIX

CONCLUSION

Conclusion

In completing this study, the objectives were evaluated for their level of completeness, and the hypothesis analyzed as either accepted or rejected. The objectives (1-5) and hypothesis (6) are re-stated here:

1. Design and integrate a coronary circulation into a previously validated *in vitro* multi-scale model [28]
2. Verify the system's response against a mathematical model
3. Validate the *in vitro* coronary blood flow against clinical findings in literature
4. Validate the entire *in vitro* model against clinical data of a HLHS patient
5. Investigate the effects of mBTS size on coronary perfusion
6. The *in vitro* model will illustrate how increased mBTS size negatively affects coronary perfusion

The present study conducted tests on a mock circulatory system of the Norwood with mBTS palliation. The MCS featured the pulmonary and systemic circulations from the Hang [28] MCS. The history of coronary modeling was investigated and led to the design of an *in vitro* coronary circulation that was implemented into the MCS, completing objective #1. A mathematical model and clinical-based literature references on CBF were used to verify the workings of the MCS and validate the coronary model, completing objectives #2 and #3. A patient-specific test (MUSC2) was used to validate

the MCS, completing objective #4. A patient-specific study that analyzed the effects of mBTS size on the Norwood, and specifically coronary, hemodynamics was conducted, completing objective #5. Thus, all five objectives were met.

In the mBTS parametric study, it was shown (see Figure 5.2) how increasing mBTS size decreases the diastolic aortic pressure. The diastolic aortic pressure is part of the coronary perfusion pressure, and so a decrease in diastolic P_{AO} leads to a decrease in coronary blood flow. Thus, a direct link between mBTS size and coronary perfusion was found, and the result was that increased mBTS size does negatively affect (by decreasing) the CBF. And so, the hypothesis is accepted.

Advantages, Disadvantages, and Future Work

The CBF was not validated against exact Norwood clinical data, but rather the best insight as to what Norwood coronary hemodynamics would be. However, in the event that clinical Norwood coronary data is obtained, the system could be operated to reflect such data. Additionally, the MCS is an open-loop system; there is no feedback to the VAD or RC components when applying distressing changes like increased mBTS size. Aortic pressure or flow is held constant in these cases to best approximate how the human body might respond. The *in vitro* MCS could be improved by adding autoregulation using a feedback-controlled system. The system could be integrated into the control of the VAD based on the flow and pressure *in vitro* measurements.

The MCS presented in this study is advantageous in that it is the first validated *in vitro* system of the Norwood palliation to feature the coronary circulation. It allowed for

verification of previous *in silico* studies through the mBTS parametric study. It can now be used to investigate other variables that would affect Norwood coronary hemodynamics, such as coarctation. Additionally, medical devices can be tested on this platform to see their effect on CBF. For instance, DeCampli et al. evaluated the use of a "counter-pulsation" device on the mBTS to improve coronary perfusion in neonatal pigs [45]. To test this device on human Norwood hemodynamics, the device could be implemented in the *in vitro* MCS. Comparison between the results obtained with and without the device would reveal its effectiveness. Hence, the presented and potential work of the *in vitro* MCS highlights the importance of an experimental setup in continuing engineering breakthroughs for single ventricle palliations.

APPENDICES

APPENDIX A: EQUIPMENT AND SYSTEM CALIBRATION

Table A.1 lists all equipment used to create the MCS and for measurement taking.

Table A.1 Equipment used in *in vivo* MCS setup and data recording.

	Equipment	Purpose
MCS	Clear PVC pipe	Compliance air chambers. Sized as needed
	Pinch-needle valves	Resistance elements
	Silicone rubber clear tubing	Connections between resistance, compliance, test section, and VAD. Sized as needed.
	Barbed tube fittings	Connect tubing to compliance air chambers
	Plastic couplings (straight, T-joint, elbow)	Connect LPN tubing
	Type 303 stainless steel hose barb	Grounding connection to LPN
	Metal wire	Grounding connection from SS hose barbs to Atrium tank and flow meters
	Ventricular-Assist Device (Excor®, Berlin Heart 25 cc, Berlin, Germany)	Create input flow to test section during pulsatile flow
	Piezo pressure regulator (Type: PRE-U2, Hoerbiger, Schongau Germany)	Control of vacuum pressure to VAD
	3-way valve (Model: 225B-111CAAA, MAC Valve, Dundee, MI, USA)	Alternate high pressure and vacuum to VAD and CC. Timing is controlled by LabVIEW.
	Pneumatic valve (at least up to10 psi)	Control of high pressure to VAD and CC
	Vacuum regulator	Control of vacuum to CC
Measurements	Electromagnetic probes (P600 series, Carolina Medical Electronics, King, NC) (30mm and 15mm circumference)	Flow measurements
	Analog Flow Meter (Model FM501, Carolina Medical Electronics, King, NC)	Flow measurements
	Pressure transducers (BD DTXplus, BD Medical Systems, Sandy, UT)	Pressure measurements
	Bridge amplifier (Model 2100, Measurements Group Inc., Raleigh, NC)	Pressure measurement's voltage nulling and amplification
	DAQ card (USB NI-6211, National Instruments) and LabVIEW software (USB 6211, LabVIEW 8.6; National Instruments, Austin, TX)	Data acquisition from pressure transducers and flow meters. Sampled at 160 Hz.
	Rigid plastic tubing and pressure taps	Connections from LPN to pressure transducers
	Vacuum and compressed air supply	VAD control

The architecture of the MCS and equipment setup is seen in Figure A.1.

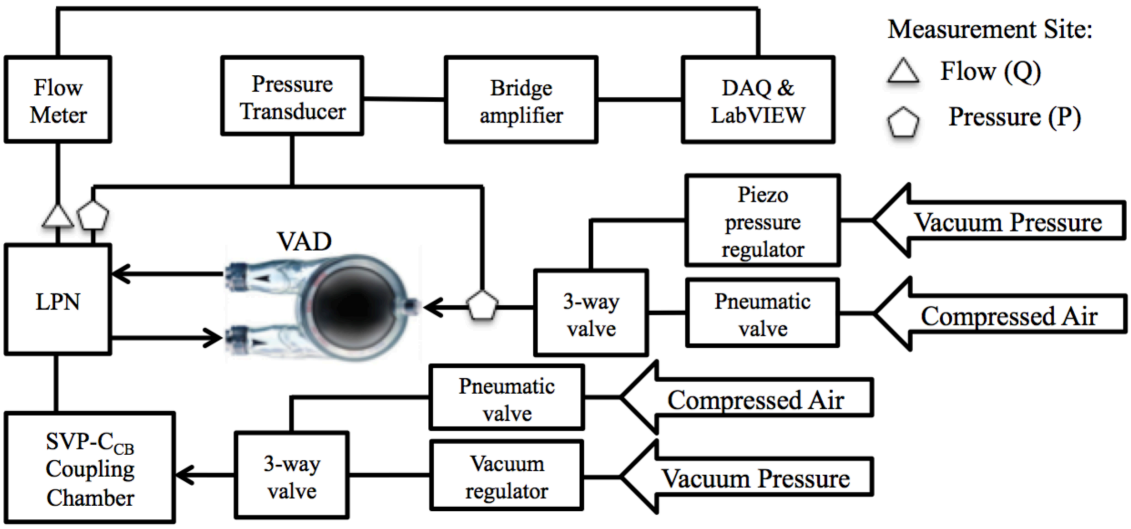

Figure A.1 Schematic of MCS and equipment setup.

The following is the step-by-step procedure for pressure transducer calibration:

1. Set the test section's ascending aorta as the datum height
2. Set all pressure taps connected to pressure transducers at the datum height
3. On the pressure transducers, set the black mark at the datum height
4. Fill a clear beaker with water and set the top of the water at the datum height
5. Connect a rigid plastic tube from the pressure transducer to the water in the beaker, ensuring that water fills the tube completely
6. With the bridge amplifier turned on and LabVIEW showing the pressure signal, adjust the amplifier's balance until the pressure reading is zero
7. Apply a known hydrostatic pressure to the beaker and adjust the amplifier's gain until the correct reading is shown on LabVIEW
8. Repeat for multiple different hydrostatic pressures and all pressure transducers

The following is the step-by-step procedure for flow meter calibration:

1. Turn on flow meter at least 30 minutes prior to use
2. Ensure all flow probes are filled with a saline solution (30 cc salt/ gallon H_2O) and there is no movement of the fluid in the probes
3. Ensure grounding wires from LPN are connected to grounding cables from flow meter
4. Ensure the flow probe's probe factor is correctly set on the flow meter by using the appropriate PFX value and *Probe Factor* dial
5. Set the *Range* dial to the range of flow appropriate to the flow
6. Turn the *Balance* dial to 500
7. With the main dial set on *OFF*, turn the *Zero* dial until the analog reading on the flow meter is zero
8. After 30 minutes and with fluid-filled probes, turn the flow meter's main dial to *Null* and adjust until the analog reading on the flow meter is at its lowest value
9. Turn the main dial to *Balance* and adjust the *Balance* dial until the reading on LabVIEW is zero
10. Turn the main dial to + and, if necessary, adjust the *Balance* dial until the reading on LabVIEW is zero
11. Measurements can now be taken with the dial set to +

The following is the step-by-step procedure for tuning the MCS to a desired test setup:

1. Ensure all flow probes and pressure transducers are calibrated prior to tuning
2. Adjust compliance air chambers to correct air volumes
3. Ensure all pressure tubing from pressure transducers to pressure taps in LPN are filled with fluid
4. Using a head tank connected directly to the LPN's C_{PROX}, set the head tank's fluid height to the hydrostatic pressure of the mean P_{AO} (This is a steady flow setup in which the VAD is disconnected and the flow from the Atrium tank is pumped up to the head tank)
5. Adjust resistance valves until the correct flows and pressures are measured in each circulation
6. Once the correct flows and pressures are tuned, disconnect the head tank setup and connect the VAD with the VAD's outflow port going towards C_{PROX} and the inflow port connected to the Atrium tank (minimize distance between each connection)
7. Ensure the air pressure connection to the VAD is disconnected and that the 3-way valve is turned on and switching back and forth between the compressed air and vacuum pressure lines (switching rate determined by systolic-time ratio designated in LabVIEW)
8. Apply compressed air and vacuum pressure to the setup
9. Slowly connect the air pressure connection to the VAD and track the pressure measurement taken between the 3-way valve and VAD. This pressure must not

fall outside the range of -80 to 250 mmHg for VAD safety. Adjustments to pressure and vacuum regulators will have to be made to apply appropriate pressure to VAD and achieve the desired mean aortic flow and pressure.

10. Get rid of any air bubbles in the MCS tubing
11. Adjust the MCS's C_{PROX} to help form the desired P_{AO} and Q_{AO}
12. Adjust the SVP's air pressure and compressed air to apply the appropriate ventricle pressure to the SVP-C_{CB} compliance chamber (CC)
13. Once the appropriate input P_{AO} is applied to the test section and the appropriate SVP applied to the CC, record the resulting pressures and flows using LabVIEW

Following the previous 13 steps, the following is the step-by-step procedure for performing a parametric test in the MCS:

14. Once the initial setup is tuned and data recorded, disconnect the air pressure from the VAD, allowing all flow to stop
15. Carefully clamp all tubing connections to the test section and remove the test section from the MCS
16. Connect another test section to the MCS. It is critical that the same position the previous test section was in is now used for the new test section and that no changes to resistance or compliance are made.
17. Unclamp tubing connections and get rid of any air bubbles
18. Repeat steps 9-13 for each new test section

APPENDIX B: ANALYTICAL MODEL

A schematic of the verification analytical model is seen in Figure B.1. For the analytical model, the inputs were the aortic pressure, aortic flow curve, and the single ventricle pressure curve. In Figure B.1, the VAD represents this implementation.

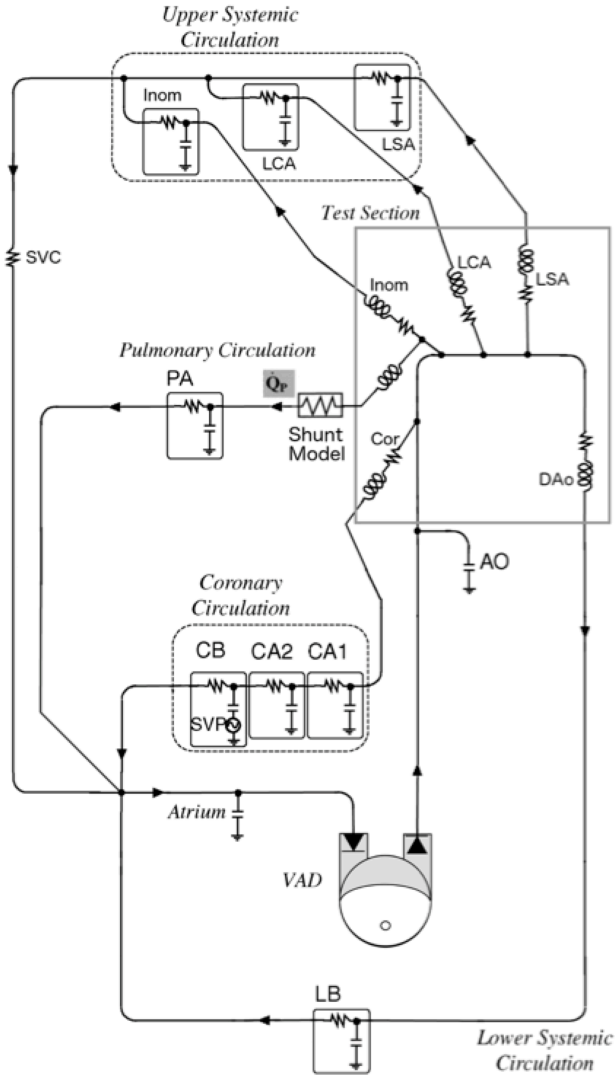

Figure B.1 Schematic of analytical model used for verification. Created by and printed with permission of Dr. Tim Conover of Clemson University.

Table B.1 shows the LPN values used in the analytical model for the verification study and Table B.2 shows the coronary LPN values used in the MUSC2 validation study.

Table B.1 LPN values used in the analytical model. Pressure (P) [mmHg], Compliance (C) [mL/mmHg], Inertance (L) [mmHg.s^2/mL], Resistance [mmHg.s/mL]

Heart		**Systemic Circulation**	
P_{Atrium}	4.1	L_{inom}	0.06919
C_{AO}	0.095	R_{inomp}	2.982
Coronary Circulation		C_{inom}	0.0888
L_{cor}	0.02801	R_{inomd}	14.517
R_{cor}	7.01	L_{lca}	0.08783
C_{ca1}	1.94E-04	R_{lcap}	2.754
R_{ca1}	10.6739	C_{lca}	0.0444
C_{ca2}	5.18E-04	R_{lcad}	31.399
R_{ca2}	10.6739	L_{lsa}	0.07724
C_{cb}	7.77E-03	R_{lsap}	2.3541
R_{cb}	32.0216	C_{lsa}	0.0444
Pulmonary Circulation		R_{lsad}	26.8339
L_{shunt}	0.04149	R_{svc}	0.586
R_{shunt}	0.461	L_{lb}	0.02276
K_{shunt}	0.14981	R_{lbp}	0.5097
C_{PA}	0.3877	C_{lb}	0.0779
R_{PA}	0.4249	R_{lbd}	7.8291

Table B.2 Coronary LPN values for the validation study. Compliance (C) [mL/mmHg], Resistance [mmHg.s/mL]

Coronary Circulation	
R_{cor}	7.71
C_{ca1}	1.71E-04
R_{ca1}	11.7413
C_{ca2}	4.57E-04
R_{ca2}	11.7413
C_{cb}	6.85E-03
R_{cb}	35.2238

APPENDIX C: STATISTICS AND UNCERTAINTY ANALYSIS

Statistics

The results of all testing were averaged over 10 cardiac cycles worth of data. A t-test at 95% confidence was used to compare mean pressure and flow results. Waveforms of MCS results and clinical or analytical results were analyzed using the coefficient of determination (R^2) (Equation C.1).

$$R^2 = \frac{N\sum_{i=1}^{N} x_i x_{ci} - \sum_{i=1}^{N} x_i \sum_{i=1}^{N} x_{ci}}{\sqrt{N\sum_{i=1}^{N}(x_i)^2 - (\sum_{i=1}^{N} x_i)^2}\sqrt{N\sum_{i=1}^{N}(x_{ci})^2 - (\sum_{i=1}^{N} x_{ci})^2}} \quad \text{(C.1)}$$

In Equation C.1, x_i and x_{ci} denote the MCS and analytical or clinical value, respectively, at the same time point in the cardiac cycle. Additionally, the waveform results were analyzed using the normalized root-mean-square error (RMSE). The normalized RMSE was calculated using range ($x_{max} - x_{min}$) and mean values ($\bar{x}$) of the result. The equations for these are seen in Equations C.2-C.4

$$RMSE = \sqrt{\sum_{i=1}^{N}(x_i - x_{ci})^2 / N} * 100\% \quad \text{(C.2)}$$

$$\sigma = \frac{RMSE}{x_{max} - x_{min}} \quad \text{(C.3)}$$

$$\omega = \frac{RMSE}{\bar{x}} \quad \text{(C.4)}$$

Uncertainty of Pressure and Flow Results

The uncertainties of mean pressure and mean flow results can be broken into systematic and random errors. Systematic error includes instrument uncertainty, zero-point error, and DAQ uncertainty. Instrument uncertainty is taken as 0.5% of the reading. Zero-point error is the difference between the true zero value and the absolute value of the minimum value achieved during zero-ing the equipment during calibration. Previous work [28] from this group found the DAQ uncertainty to be ±0.003 Lpm for flow and ±0.004 mmHg for pressure. Random uncertainty is the standard error which is found using Equation C.5.

$$S_{\bar{x}} = S_x/\sqrt{N} \tag{C.5}$$

In Equation C.5, the term S_x is the standard deviation and *N* is the number of mean values (or number of cardiac cycles the data was averaged over). The results for this thesis were averaged over N=10 cardiac cycles. The total uncertainty of the mean variable is then found using Equation C.6 where *M* stands for the total number of uncertainty terms (u_i).

$$u_{\bar{x}} = \sqrt{\sum_{i=1}^{M} u_i^2} \tag{C.6}$$

Examples of pressure and two different flow uncertainty calculations are seen in Table C.1. The smaller 15mm circumference flow probe used with the coronary flow measurements resulted in less uncertainty compared to the larger 30mm circumference

flow probe used for all other flow measurements. This was due to the smaller values of zero-point error, instrument uncertainty, and random uncertainty.

Table C.1 Example uncertainties for flow and pressure measurements. Flow uncertainty [Lpm], Pressure uncertainty [mmHg]

Name	Mean Result	Instrument Uncertainty	Zero-Point Error	Data Acquisition Uncertainty	Random Uncertainty	Total Uncertainty	Relative Value
Q_{AO}	1.7934	0.0090	0.0035	0.003	0.0357	0.037	2%
Q_{COR}	0.0545	0.0003	0.0004	0.003	0.000641	0.003	6%
P_{AO}	58.4491	0.2922	0.01	0.004	0.04	0.30	1%

Uncertainty of Resistance and Compliance Results

The uncertainties of compliance and resistance results are found using the uncertainty propagation methods as described by Figliola and Beasley [46]. The propagation of uncertainty is found using Equation C.7.

$$u_K = \left[\sum_{i=1}^{L}\left(\frac{\partial K}{\partial x_i}u_{\bar{x}_i}\right)^2\right]^{1/2} \quad \text{(C.7)}$$

In Equation C.7, u_K is the uncertainty of the result, such as resistance or compliance. The term $\frac{\partial K}{\partial x_i}$ is the sensitivity index of each variable, x_i, and $u_{\bar{x}_i}$ is the uncertainty of the variable. For resistance and compliances, such variables were pressure, flow, and air volume.

Resistance is calculated using Equation C.8 and the resulting uncertainty in resistance (u_R) is calculated using Equation C.9.

$$R = \frac{P_u - P_d}{Q} \quad \text{(C.8)}$$

$$u_R = \left[\left(\frac{1}{P_u} u_{\bar{P}_u}\right)^2 + \left(\frac{1}{P_d} u_{\bar{P}_d}\right)^2 + \left(\frac{P_d - P_u}{Q^2} u_{\bar{Q}}\right)^2 \right]^{1/2} \quad \text{(C.9)}$$

In Equations C.8-C.9, P_u and P_d are the upstream and downstream pressures, respectively. The upstream and downstream pressures were measured independently and, therefore, had no correlation between their uncertainties.

The compliance (C) and uncertainty in compliance (u_C) are calculated using Equations C.10 and C.11.

$$C = \frac{V}{P_{abs}} \quad \text{(C.10)}$$

$$u_C = \left[\left(\frac{-V}{P_{abs}{}^2} u_P\right)^2 + \left(\frac{1}{P_{abs}} u_V\right)^2 \right]^{1/2} \quad \text{(C.11)}$$

In Equation C.10 and C.11, V is the volume of trapped air in the compliance air chamber, P_{abs} is the mean absolute pressure measured at the compliance air chamber. A relative value of 1% was used for uncertainty in the volume of trapped air (u_v) such that 100mL of trapped air correlated to 1mL of uncertainty. Pressure uncertainty (u_p) was calculated using Equation C.6. Examples of resistance and compliance uncertainties are seen in Tables C.2 and C.3, respectively.

Table C.2 Example uncertainty for resistance (u_R) [mmHg/Lpm] [WU].

Resistance	P_U [mmHg]	$u_{\bar{P}_u}$ [mmHg]	P_D [mmHg]	$u_{\bar{P}_d}$ [mmHg]	*Q [Lpm]*	u_Q*[Lpm]*	u_R
UBSVR	58.6	0.3	6.02	0.06	1.27	0.01	5

Table C.3 Example uncertainty for compliance (u_C) [mL/mmHg].

Compliance	P_{abs} [mmHg]	u_P [mmHg]	*V [mL]*	u_V *[mL]*	u_C
C_{prox}	820.4	0.3	77	0.77	0.006

APPENDIX D: RESULTS

Table D.1 Mean flow, mean pressure, resistance, and compliance results for the verification study. MCS values = mean ± uncertainty

Flow [Lpm]	**Analytical**	**MCS**
Cardiac Output (Q_{AO})	1.82	1.82 ± 0.01
Upper Body (Q_{UB})	0.38	0.38 ± 0.01
Lower Body (Q_{LB})	0.4	0.40 ± 0.01
Pulmonary (Q_{mBTS})	0.98	0.98 ± 0.01
Coronary (Q_{COR})	0.056	0.056 ± 0.002
Pressure [mm Hg]	**Analytical**	**MCS**
Ascending Aorta (P_{AO})	60.11	60.37 ± 0.30
Pulmonary (P_{Pul})	11.06	11.05 ± 0.06
Lower Body (P_{LB})	56.71	57.56 ± 0.29
Innominate (P_{inom})	51.21	52.34 ± 0.28
LSA (P_{LSA})	55.91	49.68 ± 0.28
LCA (P_{LCA})	55.91	49.90 ± 0.26
Coronary CA1 (P_{CA1})	53.61	57.51 ± 0.28
Coronary CA2 (P_{CA2})	43.71	43.89 ± 0.22
Coronary CB (P_{CB})	33.8	33.61 ± 0.18
P atrium	4.1	4.1 ± 0.34
Resistance [WU]	**Analytical**	**MCS**
Upper Body (UBSVR)	148	150 ± 4
Lower Body (LBSVR)	139	140 ± 3
mBTS (R_{mBTS})	50	50 ± 1
Pulmonary (R_{pul})	7	7 ± 0.1
Total Coronary (R_{TC})	1000	1005 ± 35
Coronary Artery (R_{COR})	116	51 ± 2
Coronary CA1 (R_{CA1})	177	243 ± 9
Coronary CA2 (R_{CA2})	177	184 ± 7
Coronary CB (R_{CB})	530	527 ± 18
Compliance [mL/mmHg]	**Analytical**	**MCS**
C_{Prox}	0.095	0.094 ± 0.006
C_{Pul}	0.3877	0.374 ± 0.14
C_{LB}	0.0779	0.057 ± 0.004
C_{Inom}	0.0888	0.103 ± 0.009
C_{LCA}	0.0444	0.052 ± 0.005
C_{LSA}	0.0444	0.052 ± 0.005
C_{CA1}	0.000194351	0.00024 ± 0.00012
C_{CA2}	0.000518269	0.00050 ± 0.00013

Table D.2 Mean flow, mean pressure, resistance, and compliance results for the coronary verification study. MCS values = mean ± uncertainty

Flow [Lpm]	**Analytical**	**MCS**
Cardiac Output (Q_{AO})	1.82	1.81 ± 0.01
Upper Body (Q_{UB})	0.37	0.37 ± 0.01
Lower Body (Q_{LB})	0.4	0.40 ± 0.01
Pulmonary (Q_{mBTS})	0.98	0.98 ± 0.01
Coronary Artery (Q_{COR})	0.056	0.057 ± 0.002
Coronary Vein (Q_{CV})	0.056	0.056 ± 0.005
Coronary Artery ($Q_{COR + Rcor}$)	0.05	0.049 ± 0.002
Coronary Vein ($Q_{CV + Rcor}$)	0.05	0.047 ± 0.005
Coronary Artery ($Q_{COR ++ Rcor}$)	0.036	0.035 ± 0.002
Coronary Vein ($Q_{CV ++ Rcor}$)	0.036	0.032 ± 0.004
Pressure [mm Hg]	**Analytical**	**MCS**
Ascending Aorta (P_{AO})	60.11	60.65 ± 0.43
Coronary CA1 (P_{CA1})	53.63	54.15 ± 0.79
Coronary CA2 (P_{CA2})	43.72	43.94 ± 0.39
Coronary CB (P_{CB})	33.82	33.53 ± 0.55
Resistance [WU]	**Analytical**	**MCS**
Total Coronary (R_{TC})	1000	993 ± 34
Coronary Artery (R_{COR})	116	111 ± 2
Coronary CA1 (R_{CA1})	177	180 ± 7
Coronary CA2 (R_{CA2})	177	183 ± 7
Coronary CB (R_{CB})	530	518 ± 18
$R_{COR + Rcor}$	232	232 ± 2
$R_{COR + + Rcor}$	691	691 ± 5
Compliance [mL/mmHg]	**Analytical**	**MCS**
C_{CA1}	0.000194351	0.00025 ± 0.00012
C_{CA2}	0.000518269	0.00050 ± 0.00013

Table D.3 Mean flow, mean pressure, resistance, and compliance results for the MUSC2 validation study. MCS values = mean ± uncertainty

Flow [Lpm]	**Clinical**	**MCS**
Cardiac Output (Q_{AO})	1.26	1.25 ± 0.01
Upper Body (Q_{UB})	0.31	0.30 ± 0.01
Lower Body (Q_{LB})	0.32	0.31 ± 0.01
Pulmonary (Q_{mBTS})	0.58	0.58 ± 0.01
Coronary (Q_{COR})	0.05	0.049 ± 0.002
Pressure [mm Hg]	**Clinical**	**MCS**
Ascending Aorta (P_{AO})	58.76	58.99 ± 0.30
Pulmonary (P_{Pul})	12	12.61 ± 0.06
Coronary CA1 (P_{CA1})	52.33	51.86 ± 0.26
Coronary CA2 (P_{CA2})	42.55	41.86 ± 0.21
Coronary CB (P_{CB})	32.77	30.39 ± 0.15
Resistance [WU]	**Clinical**	**MCS**
Upper Body (UBSVR)	170	175 ± 6
Lower Body (LBSVR)	166	169 ± 6
mBTS (R_{mBTS})	80	79 ± 1
Pulmonary (R_{pul})	10	11 ± 0.2
Total Coronary (R_{TC})	1055	1073 ± 44
Coronary Artery (R_{COR})	129	144 ± 6
Coronary CA1 (R_{CA1})	196	203 ± 8
Coronary CA2 (R_{CA2})	196	232 ± 10
Coronary CB (R_{CB})	535	494 ± 20
Compliance [mL/mmHg]	**Analytical**	**MCS**
C_{Prox}	N/A	0.082 ± .006
C_{Pul}	N/A	0.29 ± .08
C_{LB}	N/A	0.081± .009
C_{Inom}	N/A	0.117± .011
C_{LCA}	N/A	0.115 ± .008
C_{CA1}	0.00017	0.00025 ± 0.00012
C_{CA2}	0.00046	0.00050 ± 0.00013

Table D.4 Mean flow, mean pressure, resistance, and compliance results for the MUSC2 mBTS-parametric study using the 3.5mm mBTS. MCS values = mean ± uncertainty

Flow [Lpm]	**Clinical**	**MCS**
Cardiac Output (Q_{AO})	1.26	1.27 ± 0.01
Upper Body (Q_{UB})	0.31	0.31 ± 0.01
Lower Body (Q_{LB})	0.32	0.32 ± 0.01
Pulmonary (Q_{mBTS})	0.58	0.58 ± 0.01
Coronary (Q_{COR})	0.05	0.051 ± 0.002
Pressure [mm Hg]	**Clinical**	**MCS**
Ascending Aorta (P_{AO})	58.76	58.63 ± 0.30
Pulmonary (P_{Pul})	12	11.96 ± 0.06
Atrium (P_{Atr})	6	6.02 ± 0.06
Coronary CA1 (P_{CA1})	52.33	52.83 ± 0.26
Coronary CA2 (P_{CA2})	42.55	43.04 ± 0.21
Coronary CB (P_{CB})	32.77	32.28 ± 0.15
Resistance [WU]	**Clinical**	**MCS**
Upper Body (UBSVR)	170.2	169 ± 5
Lower Body (LBSVR)	165.9	164 ± 5
mBTS (R_{mBTS})	80.1	80 ± 1
Pulmonary (R_{pul})	10	10 ± 0.2
Total Coronary (R_{TC})	1055	1055 ± 41
Coronary Artery (R_{COR})	129	114 ± 4
Coronary CA1 (R_{CA1})	196	193 ± 8
Coronary CA2 (R_{CA2})	196	212 ± 8
Coronary CB (R_{CB})	535	517 ± 20
Compliance [mL/mmHg]	**Analytical**	**MCS**
C_{Prox}	N/A	0.082 ± .006
C_{Pul}	N/A	0.29 ± .08
C_{LB}	N/A	0.081± .009
C_{Inom}	N/A	0.117± .011
C_{LCA}	N/A	0.115 ± .008
C_{CA1}	0.00017	0.00025 ± 0.00012
C_{CA2}	0.00046	0.00050 ± 0.00013

Table D.5 Waveform comparison results for all studies: Root-mean-square (RMS), normalized RMS (NRMS) by mean and range, and coefficient of determination (R^2).

Verification Study	**RMS**	**NRMS by mean (ω)**	**NRMS by range (σ)**	**R^2**
P_{AO}	5.21	8.6%	8.6%	0.92
Q_{COR}	0.03	52.4%	14.7%	0.83
Q_{mBTS}	0.13	13.2%	41.0%	0.83
Coronary Verification Study	**RMS**	**NRMS by mean (ω)**	**NRMS by range (σ)**	**R^2**
P_{AO}	4.957	8.2%	10.2%	0.94
Q_{COR}	0.025	44.1%	12.6%	0.87
Q_{CV}	0.033	58.8%	15.8%	0.85
Q_{COR+R}	0.022	44.6%	13.3%	0.87
Q_{CV+R}	0.034	71.5%	16.0%	0.88
Q_{COR++R}	0.011	32.0%	11.0%	0.91
Q_{CV++R}	0.030	94.5%	14.2%	0.89
MUSC2 Validation Study	**RMS**	**NRMS by mean (ω)**	**NRMS by range (σ)**	**R^2**
P_{AO}	3.98	6.7%	6.0%	0.97
Q_{mBTS}	0.07	11.3%	13.5%	0.97
Q_{AO}	0.48	38.3%	9.9%	0.92
3.5 mBTS Parametric Study Validation	**RMS**	**NRMS by mean (ω)**	**NRMS by range (σ)**	**R^2**
P_{AO}	7.02	12.0%	11.7%	0.90
Q_{mBTS}	0.05	7.8%	9.7%	0.98
Q_{AO}	0.41	32.7%	7.3%	0.97

REFERENCES

[1] B. M. Gordon, S. Rodriguez, M. Lee, and R.-K. Chang, "Decreasing Number of Deaths of Infants with Hypoplastic Left Heart Syndrome," *J. Pediatr.*, vol. 153, no. 3, pp. 354–358, 2008.

[2] S. Sano *et al.*, "Right ventricle–pulmonary artery shunt in first-stage palliation of hypoplastic left heart syndrome," no. August, 2003.

[3] The Children's Hospital of Philadelphia, "Staged Reconstruction Heart Surgery." [Online]. Available: http://www.chop.edu/treatments/staged-reconstruction-heart-surgery#.V5eIcpMrKHp. [Accessed: 24-Jul-2016].

[4] D. J. Driscoll, "Clinical Presentation and Therapy of Hypoplastic Left Heart Syndrome," pp. 637–639, 2016.

[5] F. Migliavacca, G. Dubini, E. L. Bove, and M. R. de Leval, "Computational fluid dynamics simulations in realistic 3-D geometries of the total cavopulmonary anastomosis: the influence of the inferior caval anastomosis.," *J. Biomech. Eng.*, vol. 125, no. 6, pp. 805–813, 2003.

[6] R. G. Ohye, E. J. Devaney, J. C. Hirsch, and E. L. Bove, "The modified Blalock-Taussig shunt versus the right ventricle-to-pulmonary artery conduit for the Norwood procedure," *Pediatr. Cardiol.*, vol. 28, no. 2, pp. 122–125, 2007.

[7] G. Pennati, F. Migliavacca, G. Dubini, and E. L. Bove, "Modeling of systemic-to-pulmonary shunts in newborns with a univentricular circulation: State of the art and future directions," *Prog. Pediatr. Cardiol.*, vol. 30, no. 1–2, pp. 23–29, 2010.

[8] F. Migliavacca *et al.*, "Modeling of the Norwood circulation : effects of shunt size , vascular resistances , and heart rate," pp. 2076–2086, 2007.

[9] M. Esmaily Moghadam, F. Migliavacca, I. E. Vignon-Clementel, T.-Y. Hsia, and A. L. Marsden, "Optimization of Shunt Placement for the Norwood Surgery Using Multi-Domain Modeling," *J. Biomech. Eng.*, vol. 134, no. 5, p. 51002, 2012.

[10] C. Corsini *et al.*, "The effect of modified blalock-taussig shunt size and coarctation severity on coronary perfusion after the norwood operation," *Ann. Thorac. Surg.*, vol. 98, no. 2, pp. 648–654, 2014.

[11] K. Lagana *et al.*, "Multiscale modeling of the cardiovascular system: Application to the study of pulmonary and coronary perfusions in the univentricular circulation," *J. Biomech.*, vol. 38, no. 5, pp. 1129–1141, 2005.

[12] Donnelly JP *et al.*, "Resting coronary flow and coronary flow reserve in human infants after repair or palliation of congenital heart defects as measured by positron emission tomography.," *J. Thorac. Cardiovasc. Surg.*, vol. 115, no. 1, pp. 103–110, 1998.

[13] S. Mantero, R. Pietrabissa, and R. Fumero, “The coronary bed and its role in the cardiovascular system: a review and introductory single-branch model,” *J. Biomed. Eng.*, vol. 14, pp. 109–116, 1992.

[14] Northwell Health, “Anatomy of the Heart.” [Online]. Available: https://www.northwell.edu/find-care/locations/center-aortic-disease#/figure-0-12341. [Accessed: 24-Jul-2016].

[15] D. E. L. Wilcken, “Clinical Physiology of the Normal Heart,” in *Oxford Textbook of Medicine (Volume 1)*, 4th ed., D. A. Warrell, T. M. Cox, and J. D. Firth, Eds. Oxford: Oxford University Press.

[16] D. J. Duncker and R. J. Bache, “Regulation of Coronary Blood Flow During Exercise,” pp. 1009–1086, 2008.

[17] J. D. Hutcheson, E. Aikawa, and W. D. Merryman, “Potential drug targets for calcific aortic valve disease,” *Nat Rev Cardiol*, vol. 11, no. 4, pp. 218–231, Apr. 2014.

[18] S. A. Pillai, “Understanding Anaesthesiology,” in *Understanding Anaesthesiology*, 1st ed., Jaypee Brothers Medical Publishers Ltd, 2007, pp. 230–231.

[19] D. J. R. Hildick-smith and L. M. Shapiro, “Coronary Flow Reserve Improves After Aortic Valve Replacement for Aortic Stenosis : An Adenosine Transthoracic Echocardiography Study,” vol. 36, no. 6, 2000.

[20] P. Voci, F. Pizzuto, and F. Romeo, “Coronary flow : a new asset for the echo lab ?,” pp. 1867–1879, 2004.

[21] T. Ramanathan and H. Skinner, “Coronary Blood Flow,” *Contin. Educ. Anaesthesia, Crit. Care Pain*, vol. 5, no. 2, pp. 61–64, 2005.

[22] C. Corsini, “Re: Coronary Artery Questions for In Vitro Study.” 2016.

[23] D. A. P. Part, A. M. Gaca, J. J. Jaggers, L. T. Dudley, and G. S. B. Iii, “Repair of Congenital Heart,” vol. 247, no. 3, pp. 617–631, 2008.

[24] J. M. Baffa, S.-L. Chen, M. E. Guttenberg, W. I. Norwood, and P. M. Weinberg, “Coronary artery abnormalities and right ventricular histology in hypoplastic left heart syndrome,” *J. Am. Coll. Cardiol.*, vol. 20, no. 2, pp. 350–358, 1992.

[25] J. R. Charpie, M. K. Dekeon, C. S. Goldberg, R. S. Mosca, E. L. Bove, and T. J. Kulik, “Norwood Palliation for Hypoplastic Left Heart Syndrome,” vol. 87, no. 0, pp. 0–4, 2001.

[26] B. Alsou *et al.*, “Impact of Patient Characteristics and Anatomy on Results of Norwood Operation for Hypoplastic Left Heart Syndrome,” *Ann. Thorac. Surg.*, vol. 100, no. 2, pp. 591–598, 2015.

[27] F. Migliavacca *et al.*, “Multiscale modelling in biofluidynamics : Application to reconstructive paediatric cardiac surgery,” vol. 39, pp. 1010–1020, 2006.

[28] T. Hang, “IN VITRO MULTI-SCALE PATIENT-SPECIFIC MODELING OF HEMODYNAMICS IN STAGE 1 NORWOOD PALLIATION FOR THE TREATMENT OF SINGLE VENTRICLE HEART DISEASE,” Clemson University, 2015.

[29] G. Biglino *et al.*, “Modeling single ventricle physiology : review of engineering tools to study first stage palliation of hypoplastic left heart syndrome,” vol. 1, no. October, pp. 1–9, 2013.

[30] J. Lee and N. P. Smith, “The multi-scale modelling of coronary blood flow,” *Ann. Biomed. Eng.*, vol. 40, no. 11, pp. 2399–2413, 2012.

[31] J. a. Spaan, N. P. Breuls, and J. D. Laird, “Diastolic-systolic coronary flow differences are caused by intramyocardial pump action in the anesthetized dog,” *Circ. Res.*, vol. 49, no. 3, pp. 584–593, 1981.

[32] J. M. Downey and E. S. Kirk, “Inhibition of coronary blood flow by a vascular waterfall mechanism.,” *Circ. Res.*, vol. 36, no. 6, pp. 753–760, 1975.

[33] D. A. Roberson, “Ventriculocoronary Artery Connections With the Hypoplastic Left Heart : A 4-year Prospective Study : Incidence , Echocardiographic and Clinical Features,” pp. 1176–1185, 2010.

[34] M. C. F. Geven *et al.*, “A physiologically representative in vitro model of the coronary circulation.,” *Physiol. Meas.*, vol. 25, pp. 891–904, 2004.

[35] G. M. Pantalos *et al.*, “Expanded pediatric cardiovascular simulator for research and training.,” *ASAIO J.*, vol. 56, no. 1, pp. 67–72, 2010.

[36] E. Gaillard, D. Garcia, L. Kadem, P. Pibarot, and L. G. Durand, “In vitro investigation of the impact of aortic valve stenosis severity on left coronary artery flow,” *J Biomech Eng*, vol. 132, no. 4, p. 44502, 2010.

[37] J. Calderan, W. Mao, E. Sirois, and W. Sun, “Development of an In Vitro Model to Characterize the Effects of Transcatheter Aortic Valve on Coronary Artery Flow,” *Artif. Organs*, vol. 40, no. 6, pp. 612–619, 2015.

[38] E. L. Bove *et al.*, “Use of mathematic modeling to compare and predict hemodynamic effects of the modified Blalock-Taussig and right ventricle-pulmonary artery shunts for hypoplastic left heart syndrome,” *J. Thorac. Cardiovasc. Surg.*, vol. 136, no. 2, 2008.

[39] T. Hsia *et al.*, “Management of a Stenotic Right Ventricle-Pulmonary Artery Shunt Early After the Norwood Procedure,” *ATS*, vol. 88, no. 3, pp. 830–838, 2009.

[40] P. G. and F. R., “Scaling approach to study the changes through the gestation of human fetal cardiac and circulatory behaviors.,” *Ann. Biomed. Eng.*, vol. 28, no. 4, pp. 442–452, 2000.

[41] M. Vukicevic, J. a. Chiulli, T. a Conover, G. Pennati, T.-Y. Y. Hsia, and R. S.

Figliola, “Mock Circulatory System of the Fontan Circulation to Study Respiration Effects on Venous Flow Behavior,” *ASAIO J.*, vol. 59, no. 3, pp. 253–60, 2013.

[42] N. Watanabe, S. Awa, M. Akagi, Y. Ando, and N. Oki, “Effects of heart rate and right ventricular pressure on right coronary arterial flow and its systolic versus diastolic distribution in a variety of congenital heart diseases in children,” no. January, pp. 476–482, 2000.

[43] C. Corsini *et al.*, “The Effect of Modi fi ed Blalock-Taussig Shunt Size and Coarctation Severity on Coronary Perfusion After the Norwood Operation,” 2014.

[44] P. Rasten-Almqvist, S. Eksborg, and J. Rajs, “Heart weight in infants-a comparison between Sudden Infant Death Syndrome and other causes of death,” pp. 1062–1067, 2000.

[45] W. M. DeCampli, V. Secasanu, I. R. Argueta-Morales, K. Cox, C. Ionan, and A. J. Kassab, “External Counterpulsation of a Systemic-to-Pulmonary Artery Shunt Increases Coronary Blood Flow in Neonatal Piglets,” *World J. Pediatr. Congenit. Hear. Surg.*, vol. 6, no. 1, pp. 75–82, 2015.

[46] R. S. Figliola and D. E. Beasley, *Theory and Design for Mechanical Measurements*, 5th ed. .